NASA Technical Memorandum 81782

Preliminary Results of Simulated Vortex Encounters by a Twin-Engine, Commercial Aircraft During Final Landing Approach

Earl C. Hastings, Jr., G. Thomas Holbrook,
and Gerald L. Keyser, Jr.

MAY 1980

National Aeronautics and
Space Administration

Langley Research Center
Hampton, Virginia 23665

SUMMARY

Piloted simulations of encounters with vortices of various ages and degrees of attenuation have been performed with the Visual Motion Simulator at the Langley Research Center. In the simulations, a twin-engine, commercial transport on final approach, encountered the modeled vortices of a four-engine, wide-body, commercial transport. Unattenuated vortices (in- and out-of-ground effect) and vortices attenuated by the spoilers of the generating aircraft were used in the simulations.

The results show that the upset severity due to encounters with unattenuated vortices out-of-ground effect, decreased very little with vortex aging. The presence of ground effect, or the utilization of spoiler attenuation, had little effect on the upset severity for vortices near 45 seconds of age. The upset severity of the ground effect and 15° spoiler vortex encounters however, diminished more rapidly as the vortices aged.

The vortex induced effects which degraded landing capability were the duration of the large lateral-directional oscillations, and pitch attitude changes which caused rapid deviations in the flight path.

When encounters with unattenuated vortices occurred at an altitude of 61 m (200 ft) the landings were usually successful, although the vertical flight path deviations generally did not meet the "acceptable" criteria. Even though the initial upset severity with ground effect or with spoilers was usually less severe, the pilot was often unable to successfully complete landings when these vortices were encountered at an altitude of 30.5 m (100 ft). This was due to the shortened recovery time remaining before projected touchdown.

INTRODUCTION

The adverse effect on landing capacity of vortex imposed separation intervals between aircraft has stimulated extensive research on means of reducing these intervals. A number of potential means for reducing the vortex induced upset on a trailing aircraft (and allowing reduced intervals between aircraft) are discussed in references 1 through 5 and include attenuation by ground effect, attenuation by artificial means (such as splines or spoilers), and automatic control system design. The capability to evaluate these techniques using ground-based simulators, however, has been limited by the lack of experimental data on the characteristics of the vortex flow fields of interest.

Recent full-scale measurements of vortex characteristics have made it possible to now develop many of the flow field models required for ground based simulations. This paper presents the preliminary results of some piloted, six-degree-of-freedom, simulations which evaluate the effect of vortex

encounters on a trailing aircraft during final approach. The simulations were conducted with the Visual Motion Simulator (VMS) at the NASA Langley Research Center.

One objective of this research was to develop the capability to realistically simulate piloted aircraft vortex encounters. Additional objectives were to show the effects of vortex age and attenuation on the severity of the initial upset, and to define the vortex induced effects which adversely effect recovery and landing capability after the initial upset.

SYMBOLS AND ABBREVIATIONS

Values are given in SI and U.S. Customary Units. Measurements were taken in U.S. Customary Units.

a	coefficient used in vortex model equations
AR	wing aspect ratio, b^2/S
b	wing span, m
b_1, b_2	line segment intercepts (at r = 0) used in vortex model equations, m
$\bar{c}$	wing mean aerodynamic chord, m
C_l	rolling moment coefficient, $\frac{\text{rolling moment}}{qSb}$, (rolling moment to the right is positive)
C_L	lift coefficient, $\frac{\text{lift}}{qS}$
C_m	pitching moment coefficient, $\frac{\text{pitching moment}}{qS\bar{c}}$, (nose up moment is positive)
C_n	yawing moment coefficient, $\frac{\text{yawing-moment}}{qSb}$, (nose right moment is positive)
f(Rn)	Reynolds number function
h	altitude with respect to ground level, m
$\Delta h_{G.S.}$	vertical displacement from glide slope, positive above the glide slope, m
KIAS	knots indicated airspeed
m_1, m_2	line segment slopes used in vortex model equations, per second
q	free-stream dynamic pressure, Pa
r	radial distance from the vortex centerline, m

r_c	radial location at which $V_{tan_{max}}$ occurs; vortex core radius, m
r_1, r_2	radial locations used in vortex model equations, m
S	wing reference area, m^2
t	time, sec
T	vortex age, sec
V	velocity, knots or m/sec
V_{tan}	vortex tangential velocity, m/sec
X	longitudinal distance from the projected touchdown point (positive prior to the glide slope projected touchdown point), m
Y	lateral distance from the extended runway centerline, (positive to pilot's right side), m
α	angle of attack (nose up is positive), deg
β	angle of sideslip (nose left is positive), deg
δ_a	aileron position (left aileron up is positive), deg
δ_e	elevator position (trailing edge down is positive), deg
θ	body pitch attitude (nose up is positive), deg
ν	kinematic viscosity, m^2/sec
ϕ	roll angle (right wing down is positive), deg
$\dot{\phi}$	roll rate (right roll is positive), deg/sec

Subscripts

E	vortex encounter
i	indicated
max	maximum
TD	touchdown
TH	threshold
∞	free-stream

DESCRIPTION OF THE SIMULATION

Simulator

The Visual Motion Simulator (VMS) used in this study is described in detail in reference 6. A photograph is shown in figure 1. The VMS is a six-degree-of-freedom, motion base simulator capable of presenting realistic acceleration and attitude cues to the pilot. Audio cues for throttle and aerodynamic buffet are also provided. The simulator cockpit is of standard transport aircraft design with pilot and copilot stations. Pilot controls include the standard control-wheel, pedals, and right hand throttle. Aircraft attitude display information is provided with localizer and glide slope pitch/roll command bars. Other instrumentation included indicated airspeed, vertical airspeed, and altitude.

The Visual Landing Display System (VLDS) shown in figure 2 provides the pilot a color, out-the-window scene of the simulated flight. The system utilizes an 18 m by 7.3 m (60 ft by 24 ft) three-dimensionally scaled terrain model, including a large commercial airport, which is traversed in three axes by a gantry carrying a closed circuit color television. Gantry movements account for aircraft latitude, longitude, and altitude while the television optics system motions account for heading, pitch, and bank of the aircraft. Camera and gantry motions are commanded by the aircraft simulation computer program and the resulting scene is routed to the window screen of the VMS.

Computer Program

Real-time simulations had previously been conducted in the VMS for the Boeing 737-100 aircraft shown in figure 3. (Descriptions of these simulations and some of the aircraft characteristics used in the simulations are given in refs. 7 and 8.) Because of this prior simulation experience, and since this is a typical commercial jet transport as well, the 737-100 was used as the simulated aircraft in this investigation. Therefore, it was necessary only to write a subroutine which imposed vortex induced forces and moments on the existing program. This was done using the strip theory technique described in detail in reference 5.

In summary, the technique of reference 5 involved dividing the wing, horizontal tail, and vertical tail into chordwise strips and proceeding through the following steps:

(1) start with known aircraft location (defined by center of gravity) and attitude,

(2) select strip to be considered,

(3) define location of point on desired strip in body axis system,

(4) transform location of desired point to earth fixed axis system,

(5) compute two-dimensional earth-referenced flow at point of interest in space due to both vortices,

(6) transform earth-referenced flow at point of interest to body axis system in aircraft,

(7) compute incremental, angle of attack and sideslip on desired strip,

(8) compute incremental force on strip (due to vortex flow),

(9) repeat steps 2 through 8 for each strip,

(10) sum the forces and moments for each strip,

(11) add forces and moments due to vortices to forces and moments due to aircraft attitude and velocity to get total forces and moments on aircraft,

(12) integrate aircraft equations of motion over small time increments to obtain new aircraft position in space and attitude, and

(13) repeat 1 through 12 until desired time of flight is reached.

The strip theory also included the vortex effect on the fuselage side force, and pitching and yawing moments. Although the strip theory used here was the same as used in reference 5, the vortex models differed. These are described in the following section.

Vortex Models

In this investigation, four vortex models were derived for the four-engine, wide-bodied, commercial transport shown in figure 4. These models were developed from the method of reference 1 adjusted with recent measurements from full-scale vortex probes, and from ground-based measurements obtained with laser doppler radar and mono-static acoustic sensors. The procedure used in the development of these models from the measurements is described in Appendix A.

The four vortices which were modeled for this investigation are listed in Table I. The baseline vortex is the vortex of the generating aircraft in the normal landing approach configuration (leading edge slots deployed, all landing flaps at 30°, landing gear down, $C_L = 1.4$ and $V = 140$ knots). The model for the baseline vortex out-of-ground effect was derived from high altitude probes and substantiated by laser doppler data at altitudes above about 50 m. The baseline vortex in ground effect was derived from full scale ground-based measurements of the vortex at altitudes between 0 and 50 m and from towing tank measurements (see Appendix A).

The models denoted attenuated (15° spoilers) and attenuated (30° spoilers) were for the generating aircraft in the normal landing approach configuration plus spoilers number 2, number 3, and number 4 (see fig. 4) deployed at deflection angles of 15° and 30°, respectively, for vortex attenuation. (This

attenuation configuration is described in detail in ref. 4.) These models of attenuated vortices apply in or out-of-ground effect since the laser doppler measurements showed no enhanced alleviation in ground effect.

Four vortex ages, 45, 60, 90, and 120 sec, were used in each vortex model when supporting data were available. These ages represent generator-to-trailing aircraft separation distances of 1.75, 2.33, 3.5, and 4.67 n.mi., respectively, with the generator aircraft at 140 knots. Note in Table I that models for the attenuated (15° spoilers) do not exist beyond 90 sec, and models for attenuated (30° spoilers) do not exist beyond 60 sec. The laser doppler data that were used to model these conditions showed no significant flow fields beyond about 100 sec for the attenuated (15° spoilers) case or about 75 sec for the attenuated (30° spoilers) case. Data that have become available since these models were developed, indicated that 90 sec age flow fields for the attenuated (30° spoilers) vortices can exist with a velocity profile comparable to that found at the same age for the attenuated (15° spoilers) configuration. Thus, even though the investigation did not include simulated encounters of attenuated (30° spoiler) vortices at $T = 90$ secs, the results should be similar to encounters of the 15° spoilers wakes at 90 sec.

Each of the vortex models is presented graphically as an isolated semispan vortex at various ages in figures 5 and 6. The decay of the vortex with time is apparent in these figures except for the attenuated (30° spoilers) vortex model shown in figure 6(b). The best of the limited data available for this configuration showed the vortices at $T = 45$ and $T = 60$ sec to be nearly comparable, with the older vortex actually appearing stronger. Since no other data were available to clarify these models, they were utilized as shown, realizing that the true wake they represent evidently decays insignificantly between $T = 45$ and $T = 60$ sec. Thus, simulated encounter results for the attenuated (30° spoilers) model are virtually interchangeable at 45 and 60 sec.

Figure 7 gives a comparison of the velocity profiles for the four models at each test age. It is apparent that ground effect alleviation on the baseline model is more significant with increasing vortex age. Also, note that the ground effect alleviation on the baseline model is nearly comparable to alleviation achieved with the spoilers at $T = 60$ and $T = 90$ sec.

Each of the vortex models represents an isolated vortex as shed by the semispan of the generating aircraft. As shown in figure 8, the entire flow field behind the generating aircraft was simulated by superimposing two laterally spaced, contrarotating vortices of the same type and age, resulting in downwash inboard of the vortices and upwash outboard. A lateral separation of 42.1 m (138 ft) was chosen as the representative rolled up vortex spacing for all the vortex models and ages. The flow field could be positioned to allow intercepts parallel to the wake centerline at any lateral or vertical point in the field. The vortex flow field was imposed on the calm air field in lengths (along the centerline) of 122 m (400 ft).

Test Conditions and Method

Some of the dimensional and mass characteristics of the aircraft simulated in this investigation are given in Table II. The simulated aircraft was configured for the final approach with leading edge slats extended, landing flaps at 40°, and landing gear down. The stability augmentation system (automatic yaw damper) was operative at all times. The approach speed was 125 KIAS, the recommended reference speed for this flap setting at the test weight of 38,556 kg (85000 lbs). The resulting approach C_L was 1.62. Glide slope and localizer guidance were with respect to a projected touchdown point 305 m (1000 ft) beyond the runway threshold on the runway centerline.

The aircraft was initially trimmed and located for a straight-in 3° approach. The pilot's task was to make an instrument approach until the vortex was encountered, after which instruments and primarily visual cues were utilized to complete the landing if possible. A go-around was to be initiated only if the pilot believed a safe touchdown on the runway was not possible with a reasonable remaining stopping distance.

The vortex flow field could be placed at any altitude with its axis of symmetry parallel to the projected flight path. Thus, intercepts of the centerline of either left or right vortex cores could be accomplished, as well as making intercepts with a specified lateral and vertical offset from the cores. Data evaluated in this report covers only intercepts made within a 3 m radius of either core, and at altitudes of 61 m (200 ft) for the baseline out-of-ground effect vortex, and 30.5 m (100 ft) for the baseline in ground effect and spoiler attenuated vortices. Any sequence of the four vortex models (i.e., baseline, baseline in ground effect, attenuated (15° spoilers), attenuated (30° spoilers)) or ages of vortices could be run. No indication was given to the pilot of the vortex encounter altitude or the type, direction of rotation, or age of the vortex to be intercepted. Additional approach runs with no vortex field imposed were inserted into the random run sequence to insure the pilot could not anticipate the required response. Only one vortex intercept was made per run and each run combination of vortex type, age, and intercept altitude was repeated randomly up to four times.

Since the vortex flow field was imposed along 122 m (400 ft) parallel to the projected flight path, an airspeed of 125 knots resulted in a maximum encounter time of 1.9 sec. This exposure time appears realistic from flight test experience since either vortex meander, or the aircraft's response to the vortex, result in the airplane being displaced from the strong vortex core region.

The simulation was computed at 32 iterations per second, all of the data were tabulated at eight samples per second, and 16 parameters were plotted real-time during the simulation. Collected data included:

- aircraft position and attitudes
- body axis rotational rates and accelerations

- inertial accelerations
- flight path angle
- airspeed and rate of climb
- localizer and glide slope deviations
- roll, pitch, and yawing moment coefficients
- control surface and throttle motions

Additionally, following each run, pilot comments and evaluation were recorded.

RESULTS AND DISCUSSION

The preliminary results of the effect of vortex age and attenuation on initial upset severity, and the effect of vortex encounters on landing capability are presented in this section. All of these data are for encounters within 3 m of the vortex core centerline. The results of the data validation investigation are given in Appendix B.

Effect of Vortex Age and Attenuation on the Severity of the Initial Upset

The severity of the initial upset was evaluated by considering the maximum value (independent of direction) of the rolling moment coefficient ($C_{l_{max}}$), roll angle (ϕ_{max}), and roll rate ($\dot{\phi}_{max}$) imposed on the trailing airplane. The analysis of other potential intensity indicators (i.e., β, Cn_{max}, Cm_{max}) has not been completed to the point where they can be included in this preliminary report. In order to show the effect of pilot control inputs on the initial upset, both piloted and stick-fixed runs were conducted. Stick-fixed, as used in this report, allowed the automatic operation of the rudder for yaw damping. In the stick-fixed mode the airplane was trimmed for a 3^{o} approach centered with the vortex core. All of the controls remained fixed until the vortex was encountered. Thus, the stick-fixed runs were not affected by the slight (less than 3 m) lateral or vertical offsets as were the piloted runs.

Figures 9 through 12 compare the piloted and stick-fixed initial upset data for each of the vortex flow fields. Generally, the pilot control inputs had the least effect on the $C_{l_{max}}$ and $\dot{\phi}_{max}$ data. This was because these peak values were induced very quickly after the encounters. The pilot's control inputs did have a significant effect on ϕ_{max}, however. The data in these figures show that, by countering the vortex, the pilot could reduce ϕ_{max} by 25 percent to 65 percent.

Figure 13 compares the piloted initial upset data for all four vortex flow fields. The upset severity for the baseline, out-of-ground effect vortex decreases very little with vortex ages of 45 to 120 sec. The upset severity for the baseline, in-ground effect vortex is only 18 percent less than that for

the out-of-ground effect vortex at 45 sec, but the ground effect influence results in the upset severity decreasing more rapidly with vortex age. By 120 sec, the magnitudes of the in-ground effect upset parameters are less than half of those for the baseline, out-of-ground effect encounter.

In comparing the spoiler attenuated data in figure 13 with the baseline in- and out-of-ground effect data, two points should again be noted. The available laser doppler vortex velocity measurements showed no enhanced alleviation in-ground effect with spoiler attenuation and thus the initial upset data shown apply either in- or out-of-ground effect. Also, for the attenuated (30° spoilers) vortex, the increasing upset intensity with age, is to be expected based on the models utilized (see fig. 6(b)). As noted in the vortex model section, the flow field velocity data at 45 and 60 sec were comparable, implying a vortex which aged insignificantly between these ages.

In general, 15° spoiler attenuation resulted in upset severity data which were less than for the baseline out-of-ground effect, but greater than for the baseline in-ground effect. Between $T = 45$ sec and $T = 60$ sec, the 30° spoilers appear to be more effective in reducing the upset than the 15° spoilers.

Effects of Vortex Encounters on Landing Capability

In this section of the paper, two vortex induced effects which adversely affected landing capability, will be discussed using data from several typical runs for illustration.

Run 4.4 was an encounter with an attenuated (15° spoiler) vortex at $h_E = 30.5$ m. The vortex age was 90 sec and the vortex flow direction was clockwise (looking upstream). The response data are shown in figure 14. The shaded bands indicate the time period when the simulated aircraft was in the vortex flow field.

The lateral-directional response data in figure 14(a) show that, when the aircraft crossed the threshold (4.4 sec after the encounter), the vortex induced oscillations in ϕ and β had not been damped. These values were, in fact, significantly large at that time. The results show that it required about 10 sec to damp both ϕ and β. Since a normal descent and landing from 30.5 m was observed to require only about 9 sec, the duration of the vortex induced oscillations was of vital importance.

This run is typical of many runs in which the time required for the pilot to recover and damp the aircraft was greater than the time available for a normal landing. Pilot comments concerning the vortex induced lateral-directional motions were as follows:

"The β and θ errors generated when the vortex was encountered were not nearly as great as the ϕ upset. However, the β oscillations were very difficult to counter without the possibility of getting in phase with the oscillation and possibly amplifying it. The normal pilot response was to

attempt to extend the approach to gain the time necessary for natural lateral-directional stability to damp the β oscillations to near zero."

A second adverse vortex effect frequently noted in these simulations was a vortex induced change in pitch attitude. This is illustrated by the longitudinal data from Run 4.4 shown in figure 14(b). Notice in this figure that there was a significant increase in C_L following the vortex encounter. This resulted in an increase in θ which was countered by a nose down elevator input.

The result of this initial lift increase is shown by the flight path presented in figure 15. Following the encounter, the rate of descent was reduced and the flight path flattened out. This resulted in a "long" landing with touchdown at a point 622 m beyond the threshold. (Note that since h is referenced to the aircraft center of gravity in these simulations, touchdown occurred at h = 3.0 m.) Also the flight path data in figure 15 show that the lateral-directional oscillations, noted earlier, resulted in lateral displacement of the aircraft to the pilot's right of the extended runway centerline.

Vortex induced pitch oscillations are believed to be caused by lift changes on the wing which predominate over the lift changes on the horizontal tail when the aircraft is not exactly in the center of the vortex core. In Run 4.4 for example, the aircraft encountered the vortex while displaced about 1 m to the left of the center of a clockwise flow field. It is believed the nose-up pitch change resulted from the predominant upwash and increased lift on the wing and horizontal tail. Conversely, when the vortex encounter reduced the wing C_L, a nose down pitch change, and a downward deflection of the flight path followed. This effect is illustrated by the aircraft response data from Run 4.13 shown in figure 16.

In Run 4.13, the simulated aircraft encountered an attenuated (15^o spoilers) vortex at h_E = 30.5 m. The vortex age was 60 seconds and the flow direction was counter clockwise. At the encounter, the aircraft was about 3 m to the left of the vortex center. Shaded bands are again used to show when the simulated aircraft was in the vortex flow field.

The lateral-directional response data in figure 16(a) show the same large bank and sideslip excursions as the data in figure 14(a), and a Dutch roll oscillation which required about 12 sec to damp. The longitudinal response data in figure 16(b) show an initial vortex induced reduction in C_L, a resulting nose down pitch change, and a nose up elevator input. Note that the nose up elevator input was applied to counter the effect of the predominant downwash flow, and that when the aircraft flew out of the vortex influence, the pitch attitude increased to a large value of $\theta = 11.7^o$ ($\alpha = 14.5^o$).

The effect of the initial pitch down shown in figure 16(b) was to decrease the flight path angle as shown by the data in figure 17. The altitude decreased from 30.5 m at the encounter, to a value of 11 m when the aircraft crossed the threshold 4.4 sec later. Figure 17 also shows that, after this rapid rate of descent had been arrested, the pilot again landed long in order to gain time to damp the vortex induced lateral-directional oscillations. It can also be

noted that these disturbances caused the aircraft to be laterally displaced to the left of the extended runway centerline.

The pilot evaluated the vortex induced pitch effect as follows:

"The positive pitch upsets were actually somewhat of an aid to the pilot because the airplane was displaced in a "safe" direction which allowed time to null the other errors generated (assuming adequate runway length to safely land long and stop). The negative pitch upsets were quite another matter and required an immediate elevator input, particularly at the lower encounter altitude. These encounters were usually characterized by a nose down attitude, large bank angles, and a rapidly increasing rate of descent. The possibility of impacting a wing tip short of the threshold was very great. The task was further complicated because there was not enough time for the natural damping of the vortex induced oscillations to take place."

In order to provide some quantitative indication of landing capability with vortex age, all of the landings were evaluated using three criteria to which "acceptable" or "unacceptable" values were applied. These criteria were chosen merely for this preliminary evaluation and are not advanced as the most applicable criteria for use in vortex encounter simulations.

The first criteria placed allowable limits on the lateral and vertical excursions from the desired flight path following the vortex encounter. In defining the performance characteristics of flight directors for Category II approaches, reference 9 specifies limits within which the flight director shall cause the aircraft to track the indicated course, and the glide slope. These limitations, as applied to this evaluation were that at $h = 30.5$ m, Y be between ±19.5 m (±64 ft) and that $\Delta h_{G.S.}$ be between ±3.7 m (±12 ft). Although the pilot was not required to follow the flight direction commands after these encounters, these limits were used as a criteria here because they provided a quantitative evaluation of the degree of vortex induced flight path excursions.

The second criteria placed ϕ and θ attitude limits on the simulated aircraft at touchdown. The attitude limit vlaues which were used were imposed by the requirement that the nose wheel, aft fuselage, and thrust reverser actuator fairings on the simulated aircraft, all be clear of the ground at touchdown.

The third criteria placed a limit on the rate of descent at touchdown. Reference 10 defines descent velocities to be used in determining limit vertical inertia load factors for transport type aircraft. The specified limit descent velocity of 3.05 m/sec (10 ft/sec) from that reference was used as the third criteria in this evaluation.

Table III presents the results of this evaluation for the encounters with the baseline vortices, out-of-ground effect, at $h_E = 61.0$ m (200 ft). In addition to the three evaluation criteria, the distance between the threshold and the actual touchdown point (referred to as landing distance) is shown for information.

The data show that the criteria which was hardest to satisfy for the 61 m encounters, was the flight path excursion criteria. Most of these failures resulted from the aircraft being more than 3.7 m below the glide slope at the criteria altitude of 30.5 m. It is obvious from the data that increasing vortex age was not very beneficial for this criteria. This is consistent with the earlier observation that the initial severity decreased very little with age for the baseline vortex out-of-ground effect.

It can also be seen from the data in Table III that, for h_E = 61 m, the pilot was able to complete all of the landings. All of these landings met both the touchdown attitude and descent rate criteria and the landing distances were not unreasonable.

Tables IV, V, and VI present the landing evaluation from encounters with baseline vortices in ground effect, and with attenuated vortices (15^o and 30^o spoiler deflections). All of these encounters were at h_E = 30.5 m. Since, in these runs, the vortex encounter did not occur prior to reaching the altitude for evaluating flight path excursions, that criteria served no purpose and is not presented in these tables.

The results of the data in Tables IV, V and VI are all rather similar and show that, for this lower encounter altitude, the pilot was not always able to complete the landing for vortex ages less than 90 sec. Two crashes and two go-arounds are noted and one occurrence of a nose wheel hit at touchdown is also shown. After encounters with vortices 45 and 60 sec old, the landing distance frequently exceeded 609.6 m (2000 ft). The greater difficulty experienced in successfully landing after encounters at 30.5 m, results from the effect of the limited time available to stabilize the aircraft after the encounter rather than the upset severity, which was less than or equal to the upset obtained at 61 m.

CONCLUDING REMARKS

A preliminary analysis has been completed for piloted simulations of a twin-engine, commercial transport on final approach encountering the modeled vortices of a four engine, wide-body, commercial transport. The results of this analysis, which was limited to encounters near the center of the vortex core, indicate the following preliminary results.

Piloted encounters with unattenuated vortices out-of-ground effect, resulted in upset severity which decreased very gradually with increasing vortex age. The presence of ground effect, or spoiler induced attenuation, had little effect on the initial upset severity for vortices near 45 sec of age. The decrease in severity with increasing age, however, was much more rapid for encounters with the baseline vortex in ground effect or the attenuated (15^o spoilers) vortex.

The landing capability of the simulated aircraft after a vortex encounter was found to be adversely affected by large vortex induced lateral-directional oscillations which required significant time to stabilize and resulted in

long landings, and by vortex induced pitch attitude changes which caused very significant flight path excursions.

A quantitative evaluation of all of the landings showed that when unattenuated vortices were encountered at 61 m (200 ft), the vertical flight path was often deflected below designated acceptable criteria. Although the initial upset severity was usually less severe with ground effect or with spoilers, the pilot was often unable to successfully complete landings when these vortices were encountered at h_E = 30.5 m. This was due to the shortened recovery time remaining before projected touchdown. Acceptable landings after encounters at 30.5 m were usually made by landing long in order to obtain additional time to stabilize the aircraft. Some of the resulting touchdown points were more than 609.6 m (2000 ft) past the runway threshold.

APPENDIX A

DEVELOPMENT OF VORTEX VELOCITY MODELS

The capability to accurately simulate aircraft vortex encounters is dependent on the accuracy of the vortex flow field models. In the past, a lack of experimental data on the characteristics of vortices generated by specific aircraft configurations has limited the applicability of simulation studies. However, recent full-scale and towing tank measurements of vortex characteristics have made it possible to develop many of the flow field models necessary for preliminary simulation evaluations. Current vortex data do not allow development of models which take into account vortex meander (either amplitude or frequency) and turbulence (either magnitude or distribution) within the flow field.

The V_{tan} measurements were all taken behind the generating aircraft of figure 4. The full-scale measurements were obtained with (1) the ground based Laser Doppler Velocimeter (LDV) technique, (2) the ground based Monostatic Acoustic Vortex Sensing System (MAVSS) technique, and (3) flight measurements using hot wire anemometers and pitot tubes mounted on vortex probe aircraft. Each of these data systems and its inherent limitations and error sources is detailed in references 11 and 12, respectively. The full-scale, ground-based, measurements were made by the Transportation Systems Center (TSC) of the Department of Transportation, and the flight measurements were made by the Ames Research Center and the Dryden Flight Research Center of NASA. In addition to these full-scale measurements, velocity profiles from laser velocimeter measurements during a 0.01 scale towing tank investigation (ref. 2) were also used in the development of one of the vortex models. Of the full-scale data used in this analysis, only the results of the MAVSS measurements have been published (see ref. 11). The other full-scale data were made available to the Langley Research Center in preliminary form for use in developing flow fields for these simulations.

The four vortex velocity models are curve fits for the actual data measurements. The equation form of the curve was selected by examination of all runs for each generator aircraft configuration. The specific magnitudes of the vortex velocity profiles were generally selected from "worst case" runs for a given wake age and altitude. These runs had the highest velocity values over a span of about 30 m. Velocity data from either semispan were used for the models, but the models are all presented as starboard wing vortices, viewed from the rear.

The vortex models were derived from full lateral field data and reduced to an isolated semispan vortex by averaging the velocity magnitudes on either side of the vortex core at each radial station. This technique results in a conservative vortex model (stronger than actually existed) since it is only completely accurate when the opposite semispan vortex induces a constant downwash across the lateral field. The associated vortex velocity error and calculated rolling upset error on a trailing wing are negligible when the trailing wing semispan is small compared to the lateral separation of the two semispan

vortices. For the simulated vortex encounters in this study the velocity error due to this technique resulted in a calculated rolling moment coefficient error of less than 3 percent.

The full lateral flow field was produced by imposing two counter rotating vortices of the same type and age separated by 42.1 m (see fig. 8). This results in a realistic vortex wake characterized by downwash inboard of the vortices and upwash outboard.

Tables VII and VIII list the constants and coefficients for calculating each of the vortex models utilized in the simulation study. Each model is discussed in the following text.

1. Baseline, Out-of-Ground Effect

The development of this model utilized the method of reference 1 (adjusted with flight test measurements) to predict the vortex core characteristics $V_{tan_{max}}$ and r_c with vortex age, T, which differed slightly from that in reference 1. This adjusted correlation, as shown in figure 18, was used to determine r_c and $V_{tan_{max}}$.

By representing the two curves of figure 18 mathematically, taking the full-scale value of f(Rn) as 1.0, and applying the method of reference 13, it is possible to predict the flow fields at any value of T with the equations

$$V_{tan_{max}} = 9.913(C_L V_\infty)^{.5237} T^{-.4763} \tag{1}$$

$$r_c = 2.978 \times 10^{-9} \frac{(C_L V_\infty)^{1.5}}{\nu} \sqrt{T} \tag{2}$$

$$V_{tan} = V_{tan_{max}} \frac{[a \ln(r/r_c) + 1]}{r/r_c}, \text{ for } (r \geq r_c) \tag{3}$$

$$V_{tan} = V_{tan_{max}} \left(\frac{r}{r_c}\right), \text{ for } (0 \leq r \leq r_c) \tag{4}$$

The values of $V_{tan_{max}}$, r_c, and a, used for these flow fields (fig. 5(a)) are listed in Table VII-A.

APPENDIX A

This flow field prediction technique was initially verified by comparing the predictions with the flight measurements which they were attempting to match, at T = 120 sec. Good agreement was obtained. When subsequent LDV measurements by TSC became available, these independent flow field measurements were also compared with predictions at T = 45, 60, 90 and 120 sec.

This comparison showed good agreement beyond T = 90 sec. Before T = 90 sec, the LDV velocity profiles were generally offset above the predicted profiles by 0.8 to 1.5 m/sec all along the lateral field. Since the LDV data paralleled the model, the logarithmic equation form of the model, and the resulting time decay trend were validated. The model was not adjusted for the slightly higher LDV values of V_{tan} because (1) it was not known whether this difference was real or was attributable to other sources (i.e., differences in measuring system characteristics, atmospheric conditions, aircraft conditions, etc.), and (2) this difference would have only slightly increased the upset intensity.

2. Baseline, In-Ground Effect

Laser velocimeter measurements in the wake of a 0.01 scale model in a towing tank (ref. 2), and the full scale measurements in reference 11 were used in the development of this model. All of these vortex velocity data were for the vortices as they approached the ground plane. Although the full scale measurements in reference 11 were obtained with several techniques, the MAVSS measurements were the primary full-scale data for this analysis.

The flow field calculations were performed in essentially the same manner as the baseline vortex model out-of-ground effect, except that the experimentally derived vortex core characteristics differed. These vortex modeling parameters are presented in figure 19. (Note that these curves were developed only for this generating aircraft at large Reynolds numbers, and are not in the more general form used in the preceding analysis (fig. 18).)

The core characteristics in figure 19 can be mathematically represented as functions of T by the equations

$$V_{tan_{max}} = C_L V \left(1.056 \times 10^{-6} T^2 - 1.093 \times 10^{-3} T + .1403\right) \quad (5)$$

$$r_c = 4.047 \times 10^{-4} T^2 - 3.239 \times 10^{-2} T + 4.374 \quad (6)$$

Values of V_{tan} were again determined from equations (3) and (4). The values of the coefficient, a, $V_{tan_{max}}$ and r_c used to calculate the flow fields in figure 5(b), are given in Table VII-B.

This model was initially verified by again examining the match between the predicted data and the measured data from which it was derived. Good agreement was obtained at various values of T between 41 sec and 114 sec. When the unpublished LDV data were later made available by TSC, these independent data were also compared with predictions at T = 45, 60, and 90 sec (there were no LDV data available for T = 120 sec).

Generally, the LDV measured a 0.8 to 2 m smaller core radius and a 1 to 5 m/sec higher core velocity, however these differences were always confined within at least a 2 m radius of the core. It was also noticeable that, in repeated runs, the LDV did not consistently measure the same core characteristics for a given value of T, yet consistently reproduced the remainder of the velocity profile.

As a result of this comparison, the coefficient, a, for T = 60 sec (see Table VII-B) was changed to better agree with the lower values of V_{tan} from the LDV beyond the core region. However, the model was not adjusted at any vortex age to account for core region differences because of the previously noted inconsistency in the LDV values, and because velocity differences at small radii would have a minimal affect on the vortex induced rolling behavior.

3. Attenuated (15^{o} Spoilers) and Attenuated (30^{o} Spoilers)

Ground based LDV measurements were the only data available for these two particular simulated spoiler configurations on the vortex generator aircraft. Thus, the vortex models shown in figure 6 and Table VIII were based mainly on the strongest vortex measured by the LDV for the two spoiler attenuated configurations.

Generally, both of these configurations resulted in a more random and turbulent appearing tangential velocity distribution. The LDV data were available for some runs plotted as V_{tan} versus r, and other runs as an averaged cumulative circulation (ref. 11) plotted at 5 m increments from the center of the vortex. In the latter cases, an effective value of V_{tan} could be extracted between the radius stations from circulation differences between the stations. This gave an averaged velocity contour which did not reflect local flow irregularities. Therefore, due to the turbulent nature of the actual velocity contours available and lack of data runs showing detailed flow patterns, it was decided to model the tangential velocity profiles of the spoiler attenuated vortices as two or more straight line segments (see illustration with Table VIII). A drawback to this type of simple modeling is that it does not allow prediction of vortex characteristics at any value of T as is possible with the two preceding models. However, sufficient data did not exist to justify such an approach.

One important result from the LDV spoiler attenuated data is the lack of enhanced attenuation due to ground effect. A comparison of tangential velocity profiles for vortices at vastly different altitudes shows negligible differences all along the lateral field. Similar comparisons for the baseline configurations

showed much greater velocity differences, especially near the vortex core region. Therefore, the spoiler attenuated wakes were modeled the same in- or out-of-ground effect altitude.

APPENDIX B

DATA VALIDATION

Since this was the initial vortex encounter investigation using the Visual Motion Simulator, it was necessary to validate the simulator results. The validation was based on the comparisons between the simulator results and the results from other investigations which are discussed here.

In order to establish a reference value of Cl_{max}, a test was conducted in the Langley Research Center Vortex Research Facility, using the test technique described in reference 14. The test utilized 0.03-scale models of the generating and probe aircraft in the normal approach configurations. The full scale separation interval was 0.88 n.mi.

The strip theory technique of reference 5 (which was used in this simulator program) was then used to compute Cl_{max} for comparison with the reference experimental value. The vortex flow field characteristics were determined for the baseline vortex out-of-ground effect using the method described in Appendix A and referenced to the same separation interval. The computed and experimental values of Cl_{max} are compared in figure 20(a). The agreement shown by this comparison, established that the simulations gave reasonable values of Cl_{max}.

The simulator values of ϕ_{max} were next compared with the actual flight test vortex encounter data in reference 15. In the tests of reference 15, the generating and probe aircraft were the same as in the simulations, and the encounters were made with both of these aircraft in the approach configurations. The flight test ϕ_{max} data in figure 20(b) are from a flight encounter with the baseline vortex out-of-ground effect at a separation interval of 3.0 n.mi. The simulator ϕ_{max} is from figure 9 at a vortex age (T = 77.1 sec) corresponding to this separation interval.

The flight test ϕ_{max} data in figure 20(c) are from an encounter with the baseline vortex in-ground effect at a separation interval of 1.80 n.mi. The piloted simulator data are from figure 10 at a vortex age (T = 46.3 sec) corresponding to the same separation interval. The comparisons shown in figures 20(b) and 20(c) established that the piloted simulator would give reasonable bank angle values.

This result is also supported by the unpublished results of actual vortex encounters of a McDonnell-Douglas DC-9 aircraft. In these flight tests, conducted by Dryden Flight Research Center of NASA, the DC-9 aircraft probed the vortices of the generating aircraft out-of-ground effect. The general flight test technique is described in reference 12. Both the generator and probe aircraft were in the approach configurations.

Figure 20(d) compares values of ϕ_{max} for the flight test at a separation interval of 4.0 n.mi., with the simulator value from figure 9 at a vortex age (T = 103 sec) corresponding to this interval. Similarly, figure 20(e) compares

a flight value at a separation interval of 4.5 n.mi. with simulator data from figure 9 at a vortex age (T = 116 sec) corresponding to that interval. Although the flight test ϕ_{max} values are for different probe aircraft, the good agreement is felt to support the earlier conclusion, since the DC-9 and B-737 aircraft have similar wing areas and spans.

A fourth data comparison was between the time histories of ϕ, δ_a, and θ from an actual encounter (ref. 15) and from a typical simulator run (Run 3.26). The purpose of this comparison was to verify the dynamic response characteristics of the simulator data. Figure 21 shows a comparison between a real encounter in ground effect at a separation interval of 1.80 n.mi., and a simulated encounter with a vortex in ground effect at a vortex age (T = 45 sec) corresponding to a separation interval of 1.75 n.mi. The vortex flow direction relative to the pilot was clockwise in both cases.

In figure 21 the time scale from the simulator has been used and the flight data have been adjusted so that the vortex encounter occurs at approximately the same time (t = 13.5 sec) as the simulator run. It should be noted that the data beyond the first control input should not be expected to exactly agree, since the pilots, and the recovery technique were different in the two tests.

The ϕ time histories show responses in the same direction, and similar dynamic response characteristics for the initial vortex and the initial aileron inputs. The comparative δ_a time histories are quite similar following the vortex encounter. The important point to note from the comparative θ data is again, the similarity in the initial dynamic responses. As noted earlier, the magnitude and direction of θ following a vortex encounter, appears to be highly sensitive to location. Therefore the agreement shown between the direction and magnitudes of θ in this comparison, may be merely fortuitous.

REFERENCES

1. Iversen, James D.: Correlation of Turbulent Trailing Vortex Decay Data. Journal of Aircraft, Vol. 13, No. 5, May 1976.

2. Ciffone, Donald L.; and Pedley, Barbara: Measured Wake-Vortex Characteristics of Aircraft in Ground Effect. Journal of Aircraft, Vol. 16, No. 2, Feb. 1969.

3. Hastings, Earl C., Jr.; Patterson, James C.; Shanks, Robert E.; Champine, Robert A.; and Copeland, W. Latham: Development and Flight Tests of Vortex-Attenuating Splines. NASA TN D-8083, Dec. 1975.

4. Croom, Delwin R.: Low-Speed Wind-Tunnel Parametric Investigation of Flight Spoilers as Trailing Vortex-Alleviation Devices on a Transport Aircraft Model. NASA TP-1419, Apr. 1979.

5. Johnson, Walter A.; Teper, Gary L.; and Rediess, Herman A.: Study of Control System Effectiveness in Alleviating Vortex Wave Upsets. Journal of Aircraft, Vol. 11, No. 3, March 1974.

6. Parrish, Russell V.; Dieudonne, James E.; Martin, Dennis J., Jr.; and Copeland, James L.: Compensation Based on Linearized Analysis for a Six-Degree-of-Freedom Motion Simulator. NASA TN D-7349, Nov. 1973.

7. Dieudonne, James E.: Description of a Computer Program and Numerical Technique for Developing Linear Perturbation Models From Nonlinear Systems Simulations. NASA TM 78710, July 1978.

8. Parrish, Russell V.; Kahlbaum, William M., Jr.; and Steinmetz, George G.: Effect of Image Tilt of a Virtual Image Display on Simulated Transport Touchdown Performance. NASA TP-1520, Oct. 1979.

9. FAA Advisory Circular No. 120-29: Criteria for Approving Category I and Category II Landing Minima for FAR 121 Operations, Sept. 1970.

10. Airworthiness Standards: Transport Category Airplanes. Federal Aviation Regulations, Part 25.

11. Burnham, D. C.; Hallock, J. N.; Tomback, I. H.; Brashears, M. R.; and Barber, M. R.: Ground-Based Measurements of the Wake Vortex Characteristics of a B-747 Aircraft in Various Configurations. FAA Report No. FAA-RD-78-146, Dec. 1978.

12. Jacobsen, Robert A.; and Barber, M. R.: Flight-Test Techniques For Wake-Vortex Minimization Studies. In NASA SP-409, 1977.

13. Sampson, R. G.: An Experimental and Theoretical Investigation of the Structure of a Trailing Vortex Wake. Aeronautical Quarterly, Feb. 1977.

14. Patterson, James C., Jr.; and Jordan, Frank L., Jr.: Thrust Augmented Vortex Attenuation. In NASA SP-409, 1977.

15. Tracey, Peter W.: Results of Boeing Company Wake Turbulence Test Program. Boeing Document Number D6-30851.

TABLE I.- VORTEX MODELS USED IN THE INVESTIGATION

Vortex Modeled	Configuration of Generating Aircraft	Vortex Ages Modeled
Baseline, out-of-ground effect	Landing approach	45, 60, 90, 120 sec
Baseline, in-ground effect	Landing approach	45, 60, 90, 120 sec
Attenuated (15^{o} spoilers)	Landing approach plus spoilers 2, 3, and 4 at 15^{o}	45, 60, 90 sec
Attenuated (30^{o} spoilers)	Landing approach plus spoilers 2, 3, and 4 at 30^{o}	45, 60 sec

TABLE II.- CHARACTERISTICS OF SIMULATED AIRCRAFT

USED IN THE INVESTIGATION

GENERAL:		
Length, m (ft)	28.65	(94.0)
Height to top of vertical fin, m (ft)	11.28	(37.0)
WING:		
Area, m^2 (ft^2)	91.04	(980)
Span, m (ft)	28.35	(93.0)
Mean aerodynamic chord, m (ft)	3.41	(11.2)
Incidence angle, deg		1.0
Aspect ratio		9.07
Dihedral, deg		6
Sweep, deg		25
Flap area, m^2 (ft^2)	14.94	(160.8)
WEIGHT, kg (lbm)	38.556	(85000)
INERTIA, kg-m^2 (slug-ft^2)		
Roll	549,099	(405,000)
Pitch	1,080,573	(797,000)
Yaw	1,710,342	(1,261,500)
Roll-yaw product of inertia	70,841	(52,250)
CENTER OF GRAVITY, percent of mean aerodynamic chord		19

TABLE III.- LANDING EVALUATION FOR BASELINE VORTICES OUT-OF-GROUND EFFECT (h_E = 61.0 m)

Vortex age, sec	Run Number	Flt. Path Excursion	Touchdown Attitude	Descent Rate	$x_{TH} - x_{TD}$ m	$x_{TH} - x_{TD}$ ft
45	11.13	Unacceptable	Acceptable	Acceptable	224	739
	11.14	Unacceptable	Acceptable	Acceptable	247	810
	11.15	Unacceptable	Acceptable	Acceptable	327	1074
	11.16	Unacceptable	Acceptable	Acceptable	319	1046
60	S-5-28	Unacceptable	Acceptable	Acceptable	361	1186
	11.9	Unacceptable	Acceptable	Acceptable	241	792
	11.10	Acceptable	Acceptable	Acceptable	259	849
	11.11	Unacceptable	Acceptable	Acceptable	154	504
	11.12	Unacceptable	Acceptable	Acceptable	319	1045
90	11.5	Unacceptable	Acceptable	Acceptable	270	886
	11.6	Unacceptable	Acceptable	Acceptable	266	872
	11.7	Unacceptable	Acceptable	Acceptable	265	868
	11.8	Acceptable	Acceptable	Acceptable	238	782
120	9.10	Unacceptable	Acceptable	Acceptable	190	623
	9.11	Unacceptable	Acceptable	Acceptable	196	644
	9.12	Unacceptable	Acceptable	Acceptable	268	878
	9.13	Unacceptable	Acceptable	Acceptable	326	1070
	11.1	Unacceptable	Acceptable	Acceptable	342	1121
	11.2	Unacceptable	Acceptable	Acceptable	400	1312
	11.3	Unacceptable	Acceptable	Acceptable	214	703
	11.4	Unacceptable	Acceptable	Acceptable	201	660

TABLE IV.- LANDING EVALUATION FOR BASELINE VORTICES IN GROUND EFFECT (h_E = 30.5 m)

Vortex age, sec	Run Number	Touchdown Attitude	Descent Rate	$x_{TH} - x_{TD}$		Comments
				m	ft	
45	3.25	Acceptable	Acceptable	855	2805	Long landing
	3.26	Acceptable	Acceptable	682	2237	Long landing
	3.27	---	---	---	----	Crashed
	3.27R	Acceptable	Acceptable	524	1720	Long landing
60	3.18	Acceptable	Acceptable	508	1668	Long landing
	3.19	Acceptable	Acceptable	604	1982	Long landing
	3.20	---	---	---	----	Crashed
90	3.11	Unacceptable	Acceptable	379	1243	Hit nose wheel
	3.13	Acceptable	Acceptable	632	2072	Long landing
120	3.4	Acceptable	Acceptable	482	1580	Long landing
	3.5	Acceptable	Acceptable	515	1369	
	3.6	Acceptable	Acceptable	459	1506	Long landing

TABLE V.- LANDING EVALUATION FOR ATTENUATED (15° SPOILER) VORTICES (h_E = 305. m)

Vortex age, sec	Run Number	Touchdown Attitude	Descent Rate	$x_{TH} - x_{TD}$		Comments
				m	ft	
45	4.18	Acceptable	Acceptable	865	2837	Long landing
	4.19	---	---	---	----	Go-around
	4.20	---	---	---	----	Go-around
60	4.11	Acceptable	Acceptable	637	2091	Long landing
	4.12	Acceptable	Acceptable	632	2073	Long landing
	4.13	Acceptable	Acceptable	859	2818	Long landing
90	4.4	Acceptable	Acceptable	622	2040	Long landing
	4.5	Acceptable	Acceptable	538	1764	Long landing
	4.6	Acceptable	Acceptable	476	1563	Long landing

TABLE VI.- LANDING EVALUATION FOR ATTENUATED (30° SPOILERS) VORTICES (h_E = 30.5 m)

Vortex age, sec	Run Number	Touchdown Attitude	Descent Rate	$x_{TH} - x_{TD}$		Comments
				m	ft	
45	5.11	Acceptable	Acceptable	843	2767	Long landing
	5.12	Acceptable	Acceptable	450	1475	
	5.13	Acceptable	Acceptable	641	2104	Long landing
60	5.4	Acceptable	Acceptable	678	2224	Long landing
	5.5	Acceptable	Acceptable	770	2527	Long landing
	5.6	Acceptable	Acceptable	777	2549	Long landing

TABLE VII.- CONSTANTS AND COEFFICIENTS FOR BASELINE VORTEX MODELS

A. OUT-OF-GROUND EFFECT			
T (sec)	r_c (m)	$V_{tan_{max}}$ (m/sec)	a
45	1.250	18.23	.92939
60	1.402	15.70	.92939
90	1.737	12.92	.92939
120	2.012	11.43	.92939

B. IN GROUND EFFECT			
T (sec)	r_c (m)	$V_{tan_{max}}$ (m/sec)	a
45	3.719	9.479	.92939
60	3.962	8.534	.78720
90	4.663	5.151	.92939
120	6.340	2.530	.92939

TABLE VIII.- CONSTANTS AND COEFFICIENTS FOR ATTENUATED VORTEX MODELS

A. 15^{o} Spoilers								
T (sec)	r_c (m)	$V_{tan_{max}}$ (m/sec)	r_1 (m)	m_1 (sec^{-1})	b_1 (m/sec)	r_2 (m)	m_2 (sec^{-1})	b_2 (m/sec)
45	1.3716	13.716	7.620	-.9756	15.054	49.179	-.1833	9.016
60	1.3716	8.8392	33.263	-.2772	9.2202	33.263	0	0
90	1.3868	6.6690	31.038	-.2249	6.9799	31.038	0	0

B. 30^{o} Spoilers								
T (sec)	r_c (m)	$V_{tan_{max}}$ (m/sec)	r_1 (m)	m_1 (sec^{-1})	b_1 (m/sec)	r_2 (m)	m_2 (sec^{-1})	b_2 (m/sec)
45	2.0269	6.8153	21.336	-.07348	6.9647	60.96	-.1362	8.3028
90	0.9327	7.4981	21.336	-.08626	7.5773	60.96	-.1448	8.8270

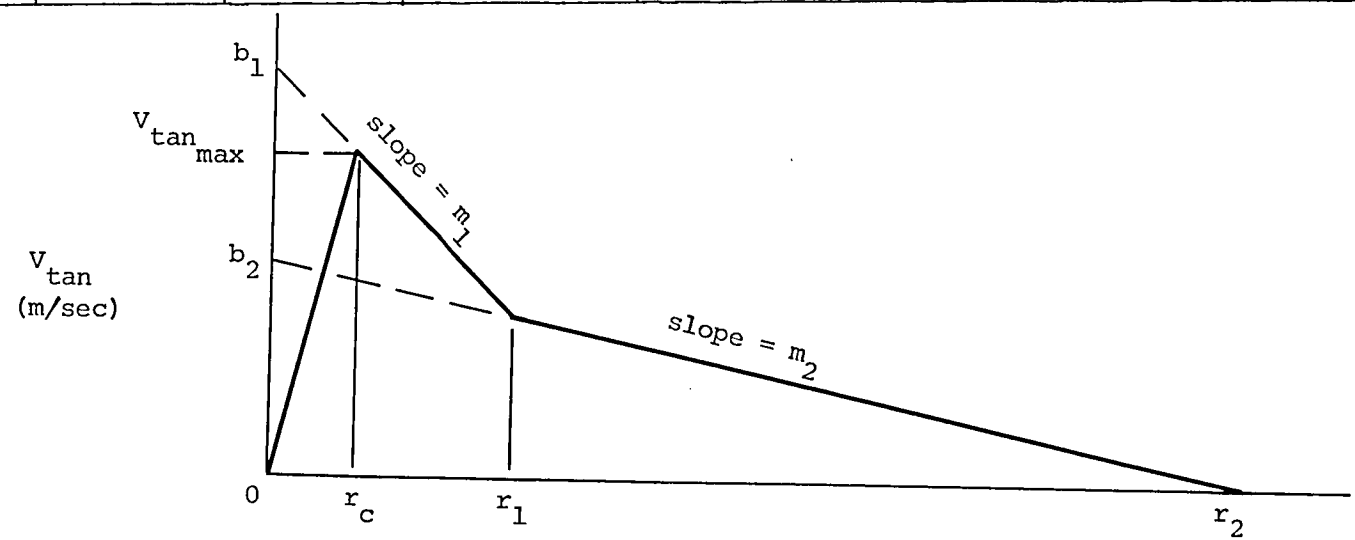

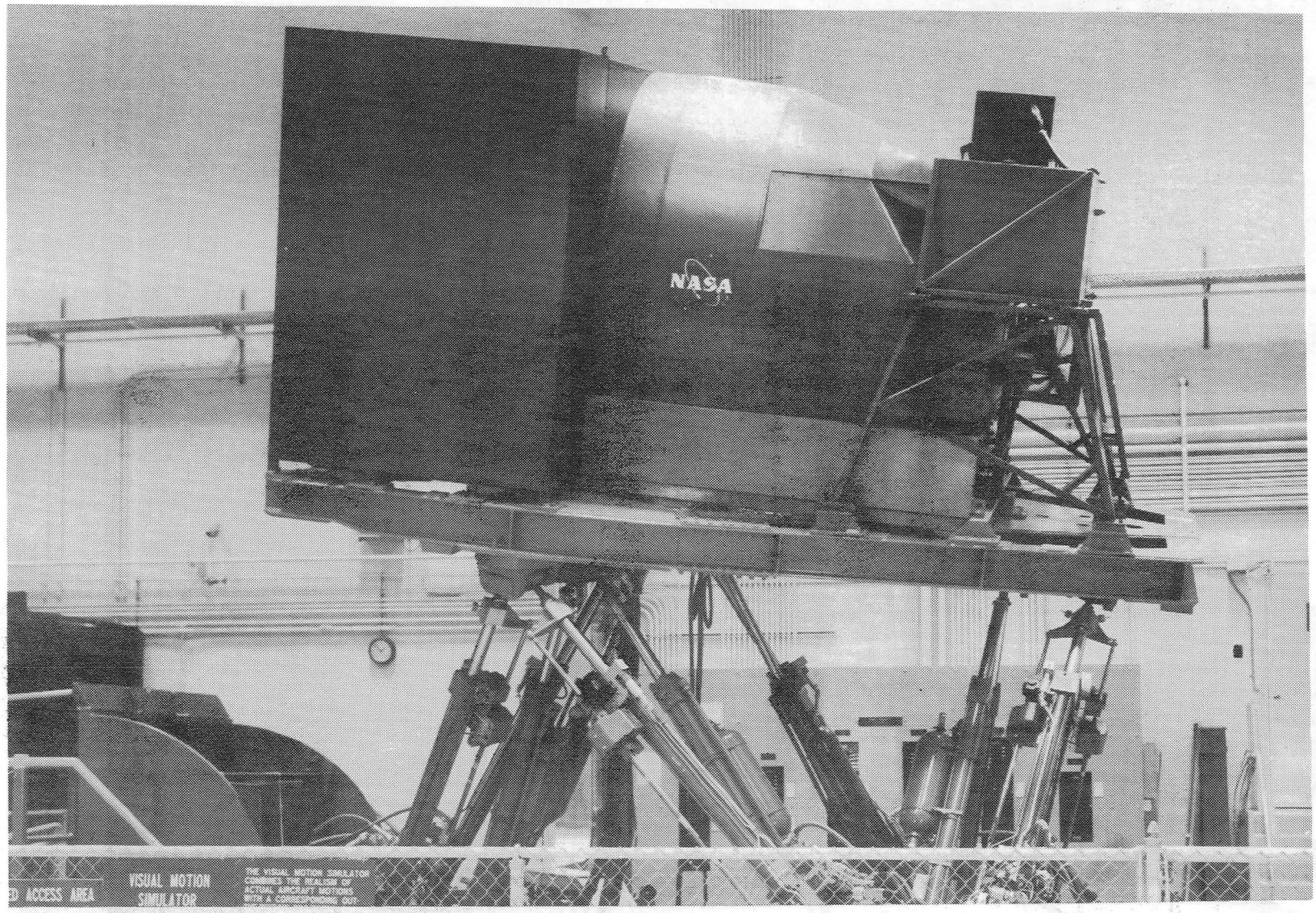

Figure 1.- Photograph of the Visual Motion Simulator.

Figure 2.- Photograph of the Visual Landing Display System.

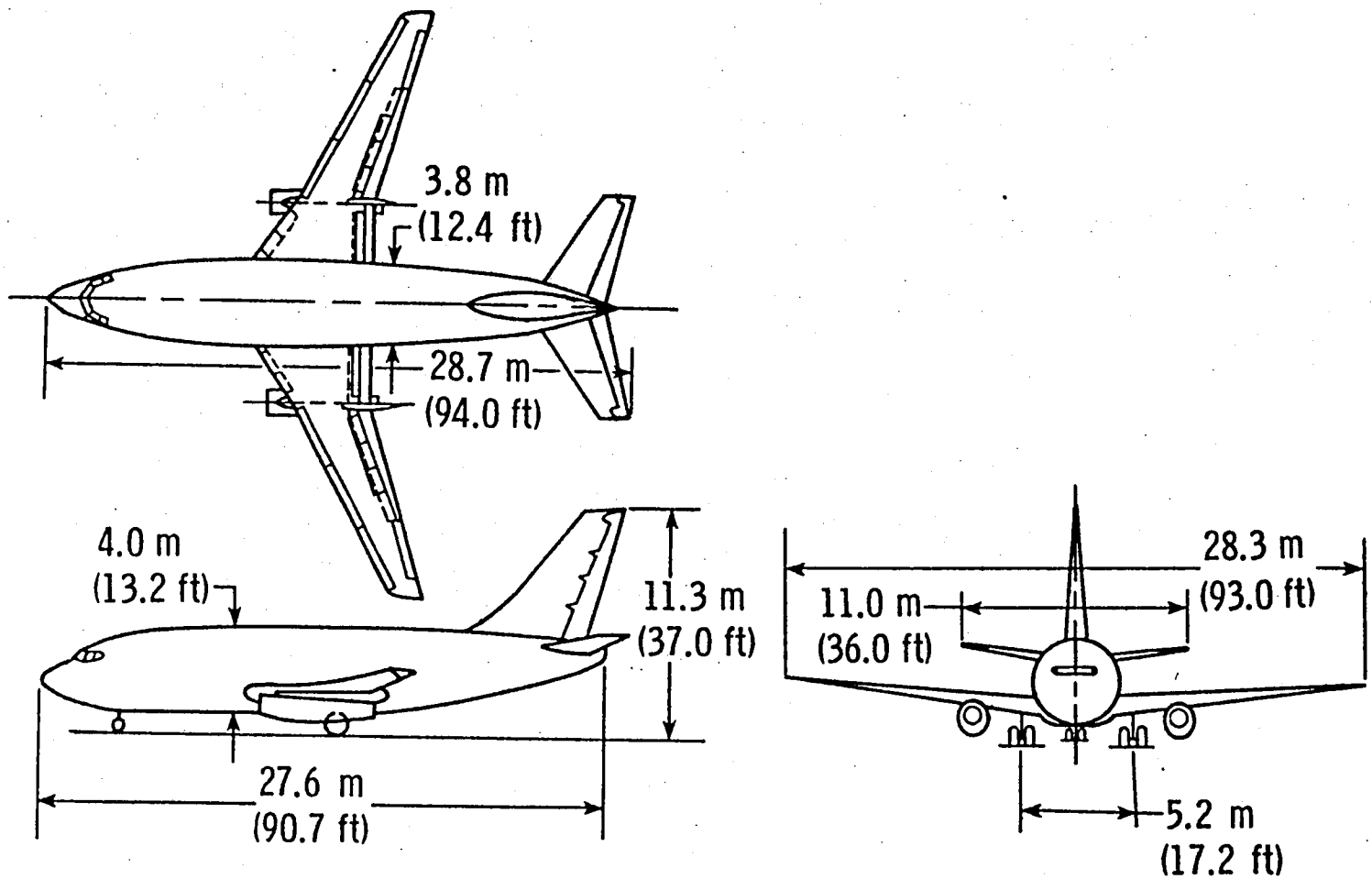

Figure 3.- Sketch of the Boeing 737-100 aircraft simulated in the investigation.

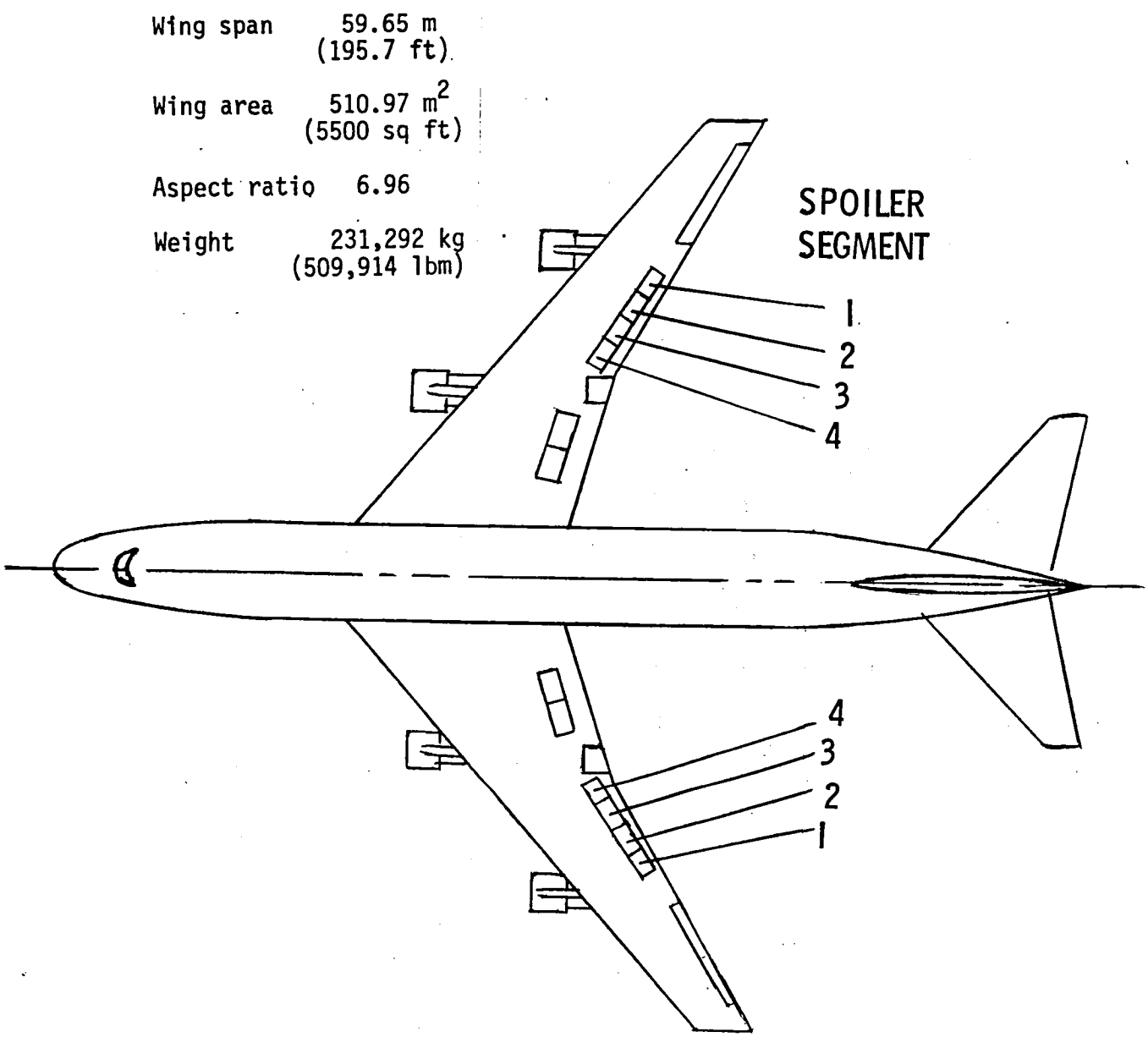

Figure 4.- Drawing of the vortex generating aircraft used in the investigation.

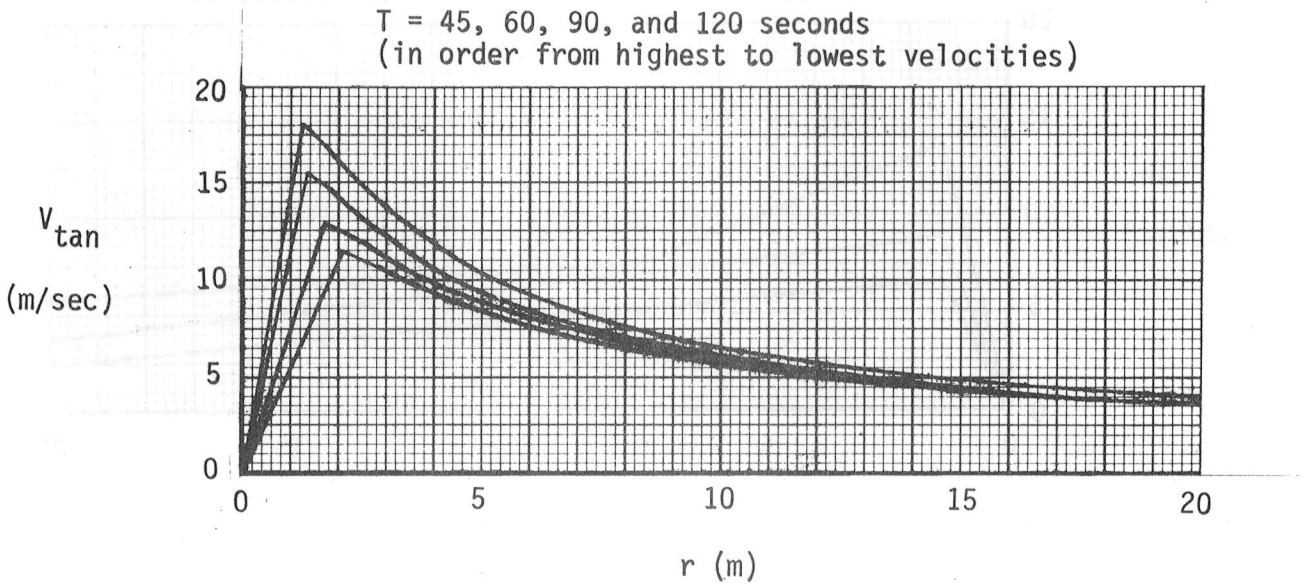

(a) Baseline, out of ground effect.

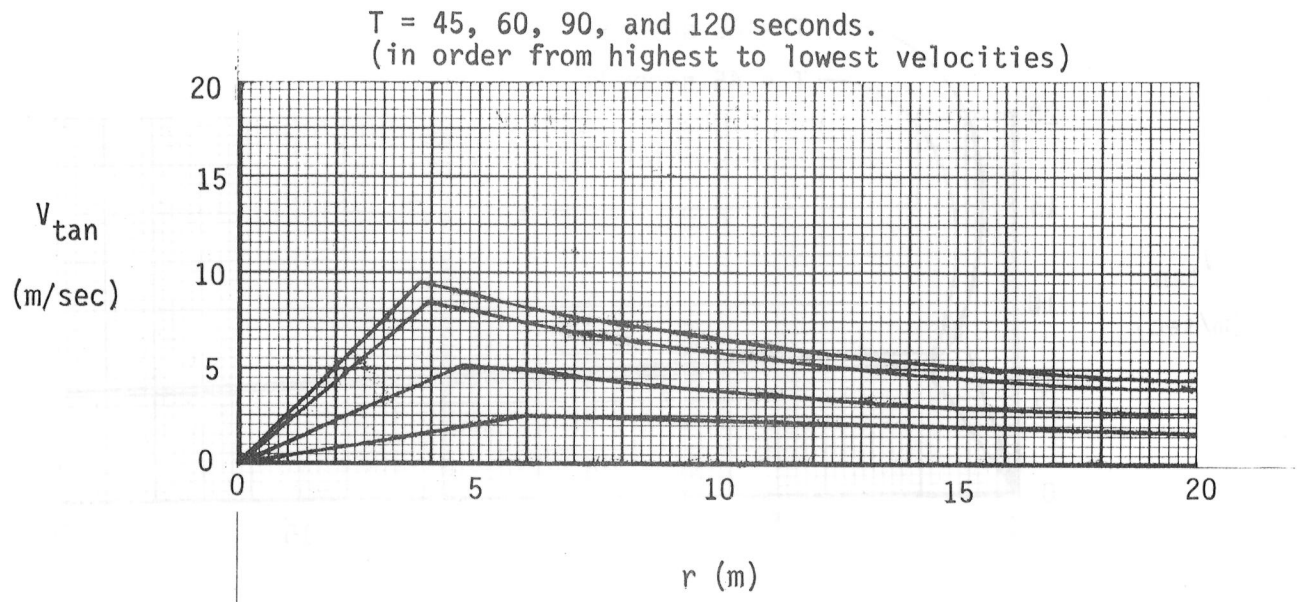

(b) Baseline, in ground effect.

Figure 5.- Baseline vortex model.

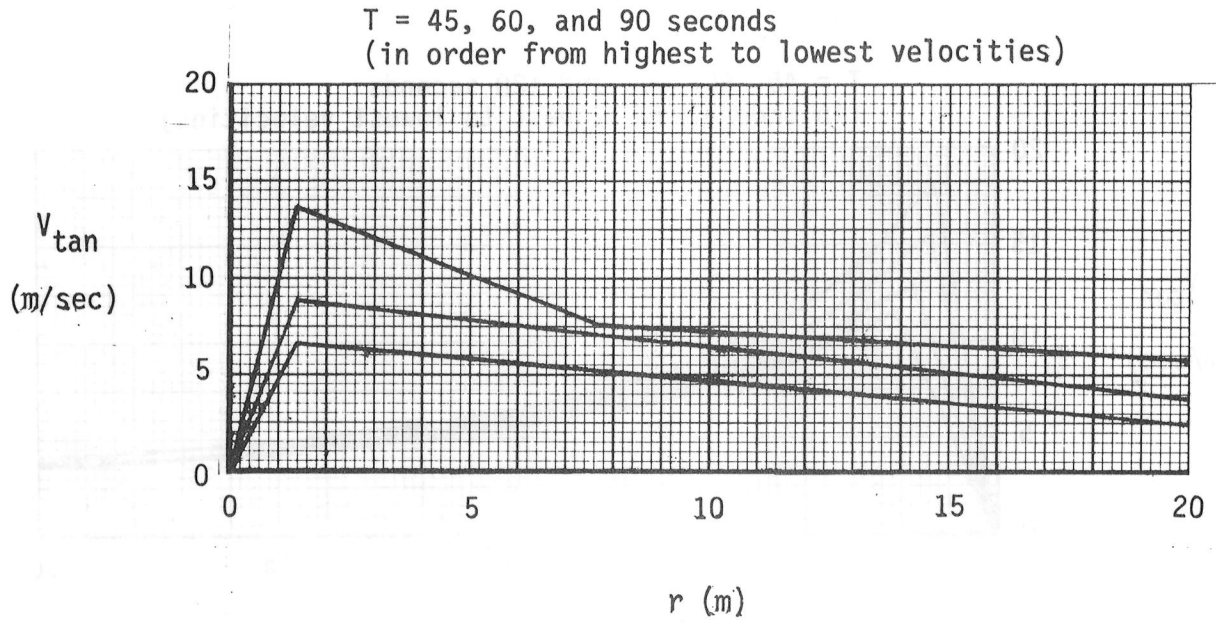

(a) Attenuated (15^{o} spoilers).

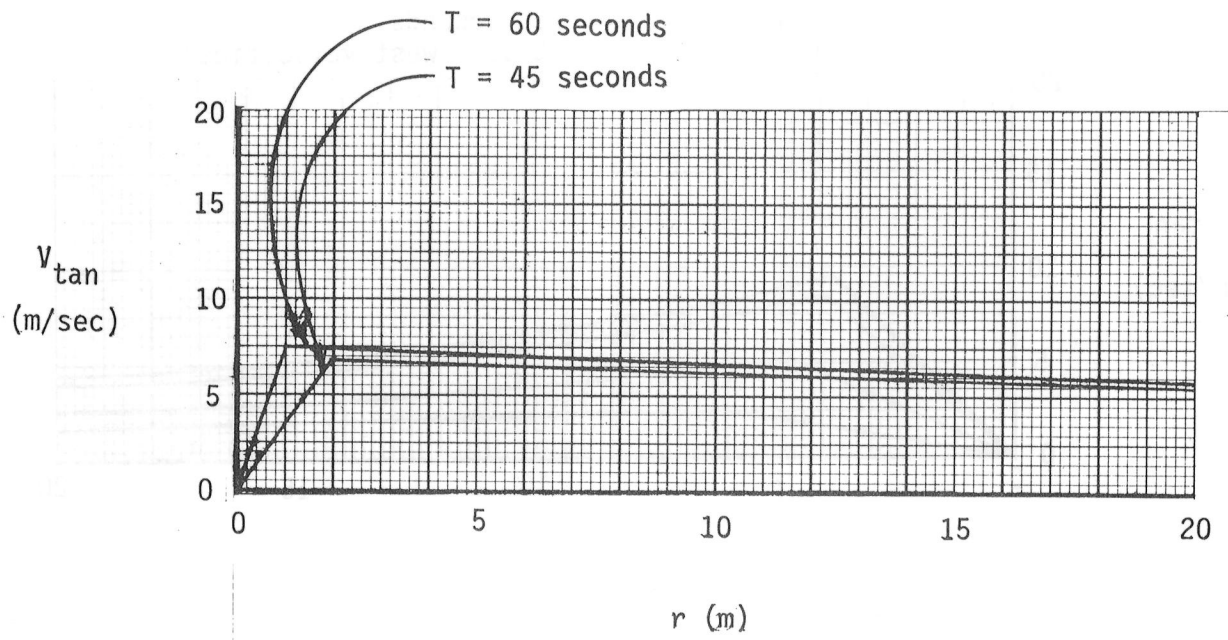

(b) Attenuated (30^{o} spoilers).

Figure 6.- Spoiler attenuated vortex models.

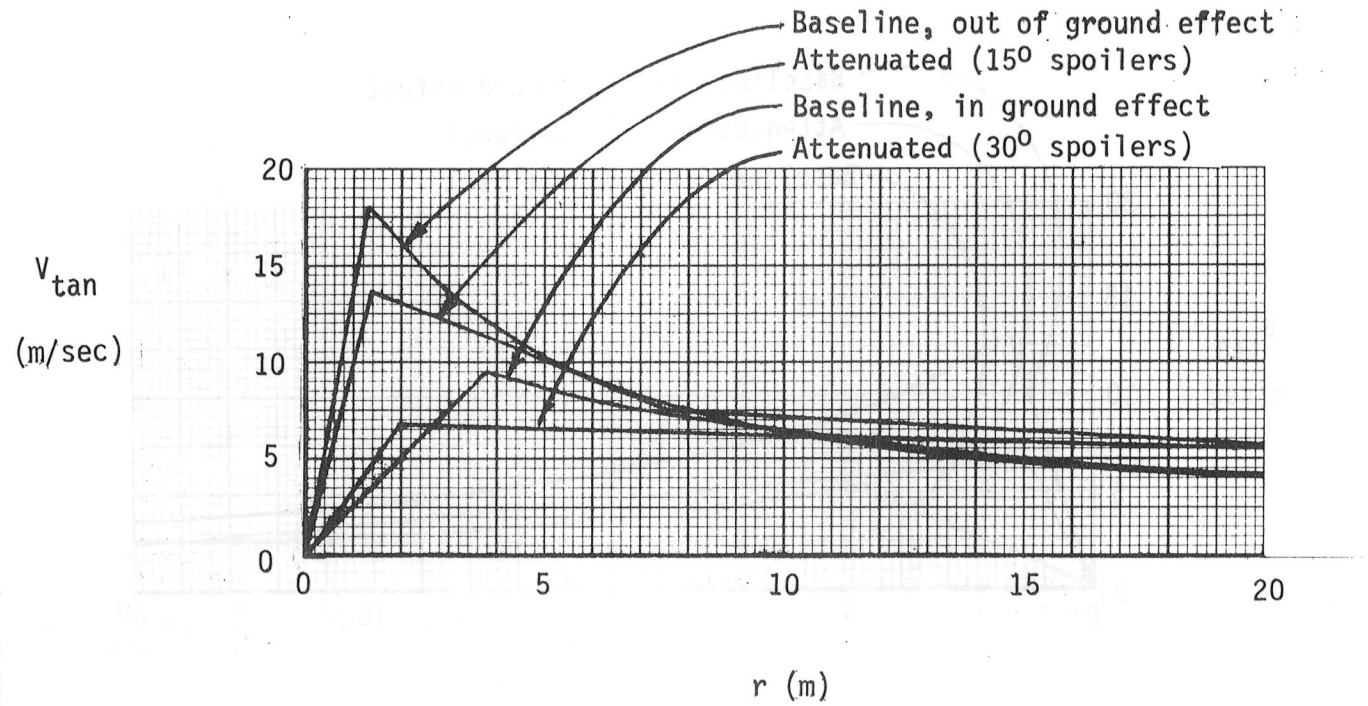

(a) T = 45 seconds.

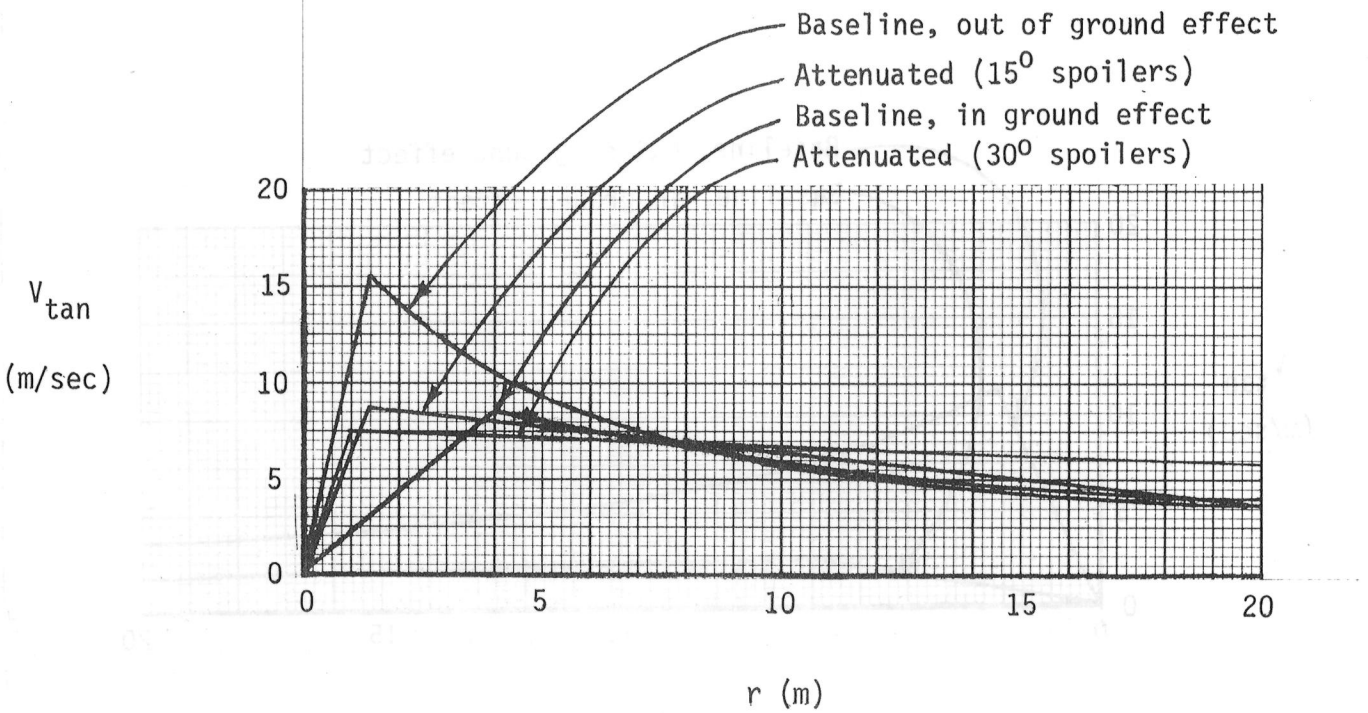

(b) T = 60 seconds.

Figure 7.- Comparison of vortex models from T = 45 seconds to T = 120 seconds.

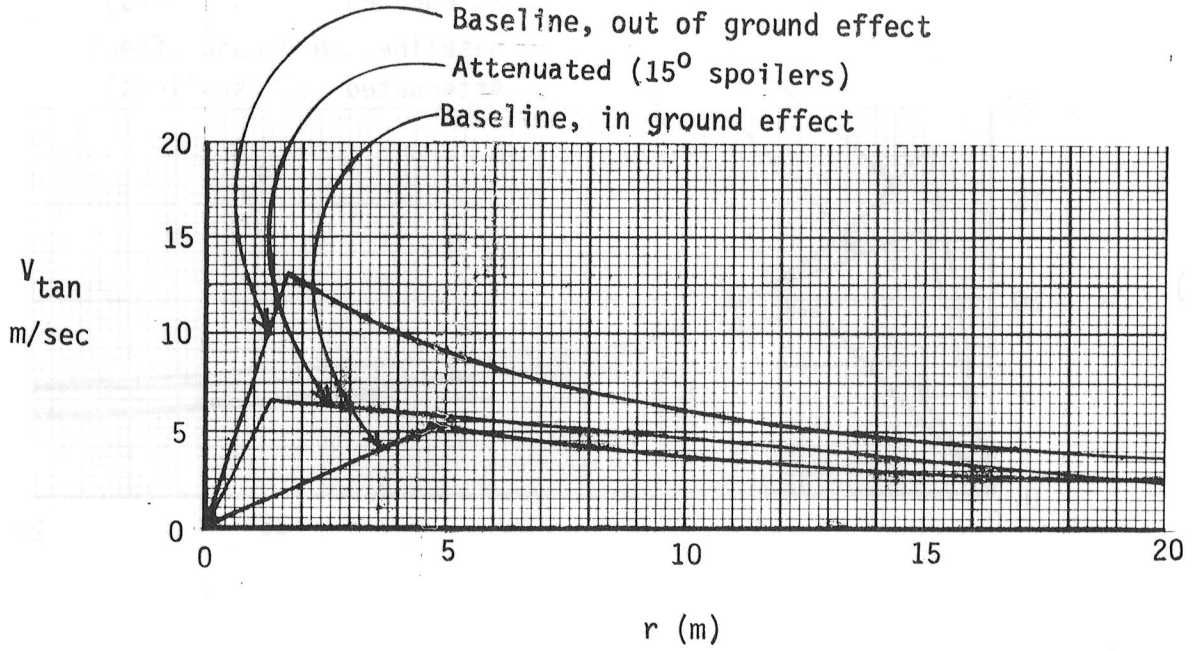

(c) T = 90 seconds.

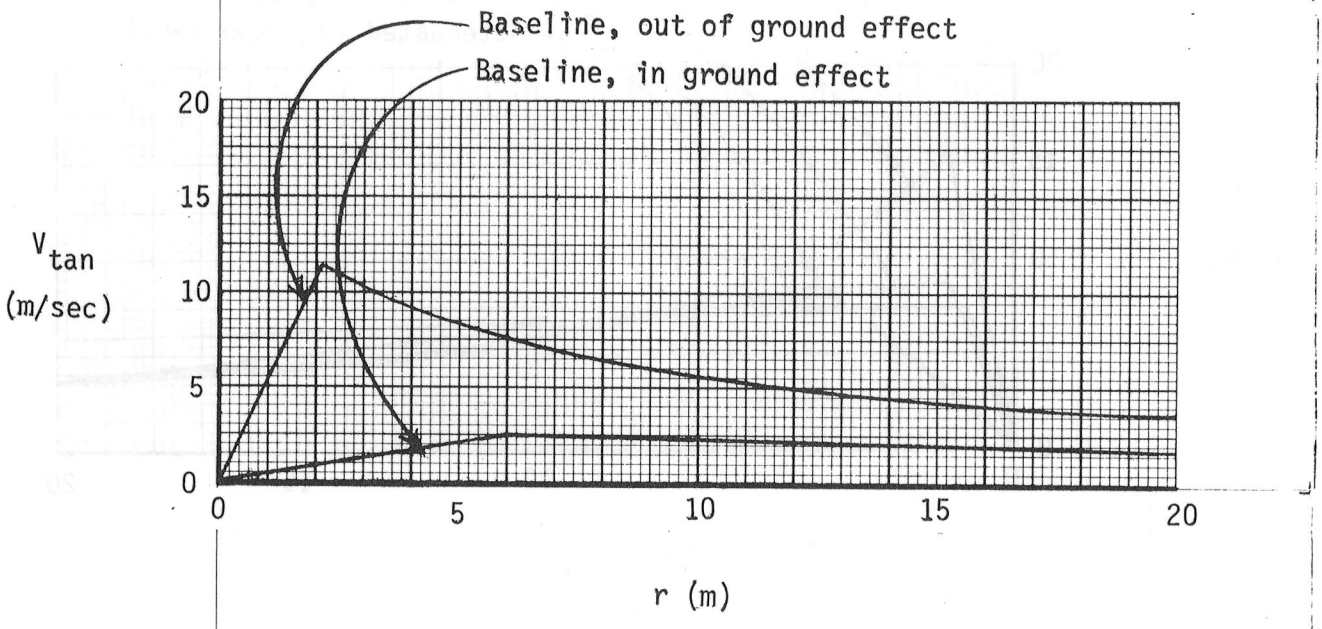

(d) T = 120 seconds.

Figure 7.- Concluded.

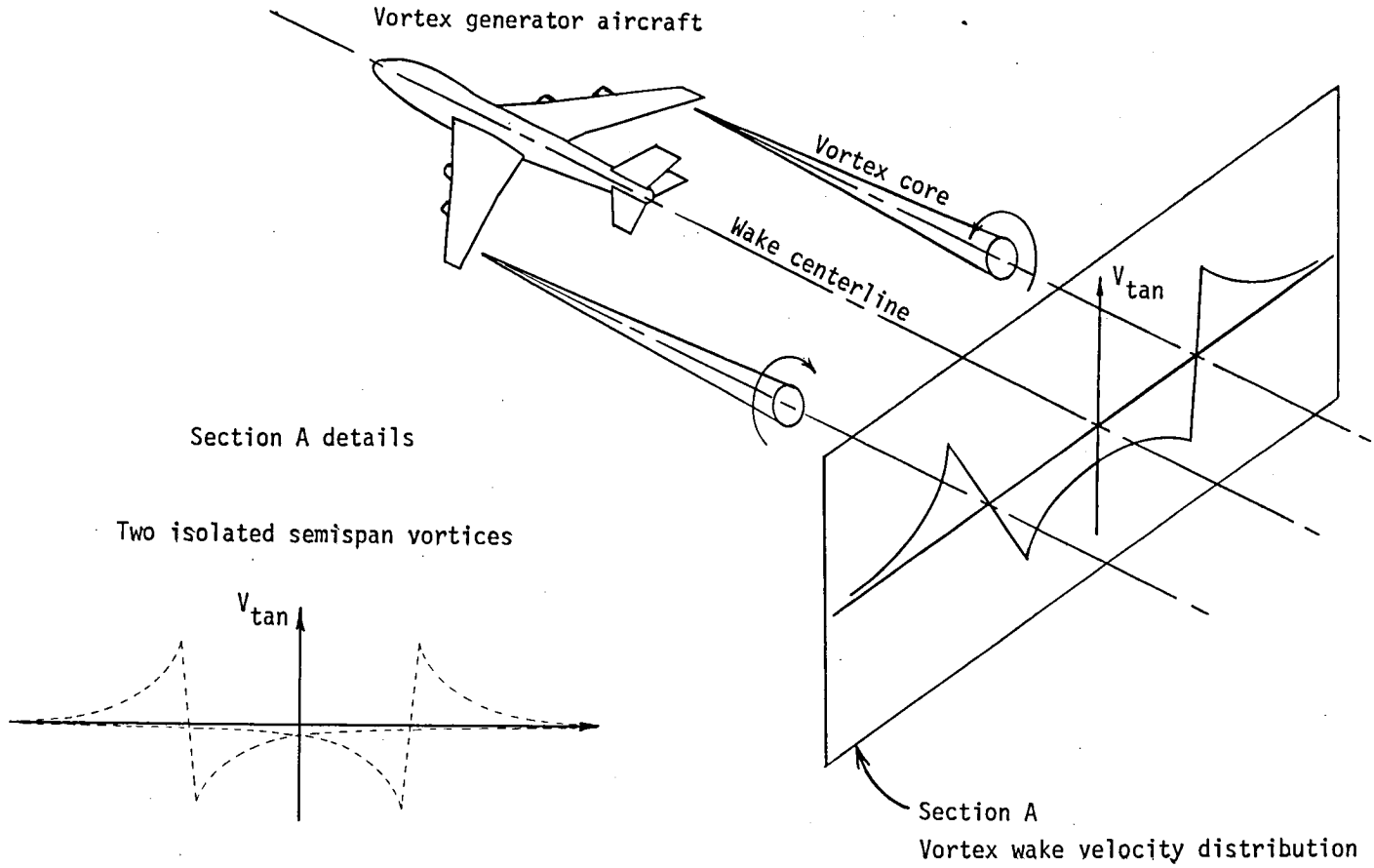

Figure 8.- Simulated flow field.

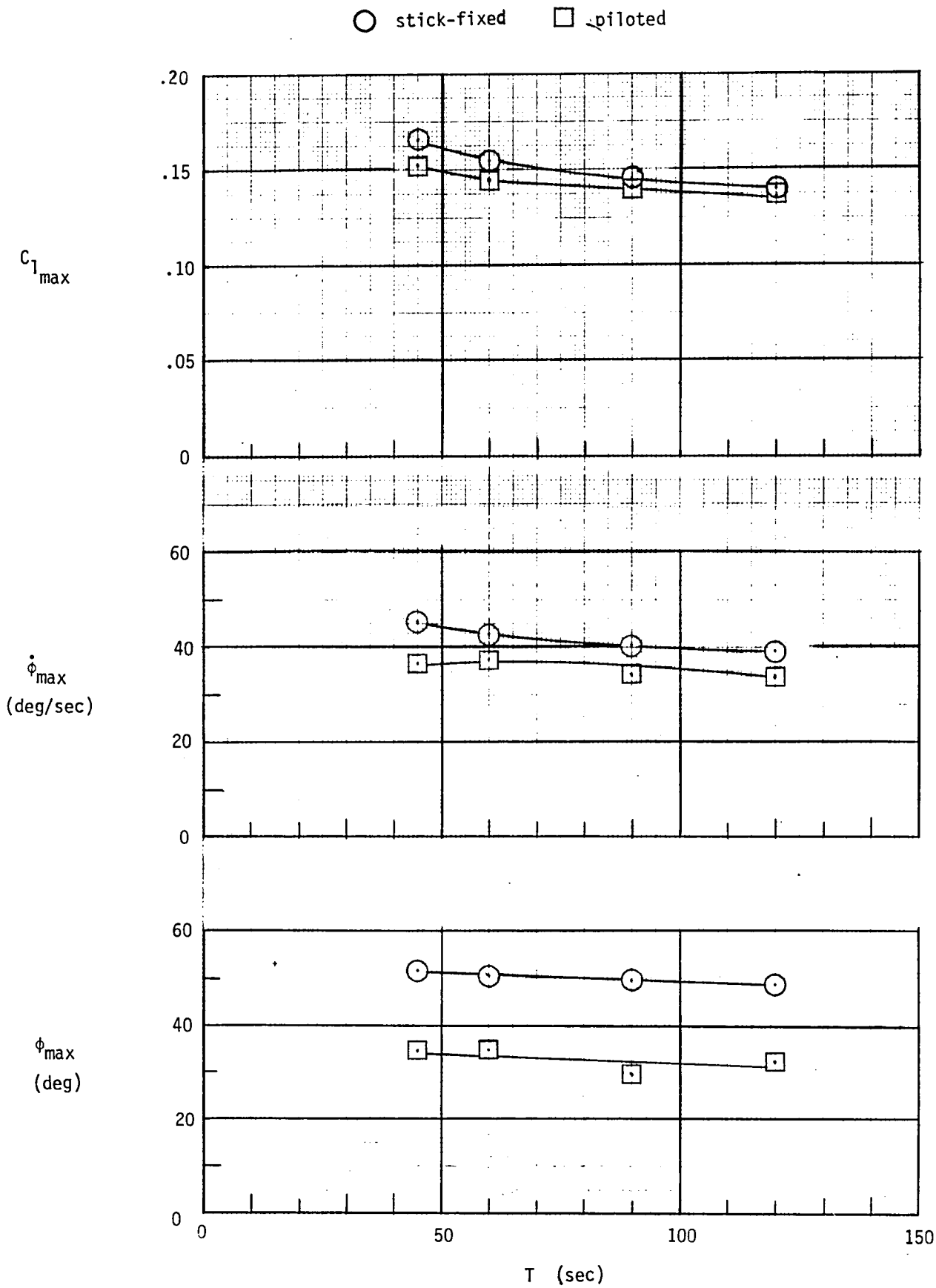

Figure 9.- Initial upset severity from baseline, out of ground effect vortices.

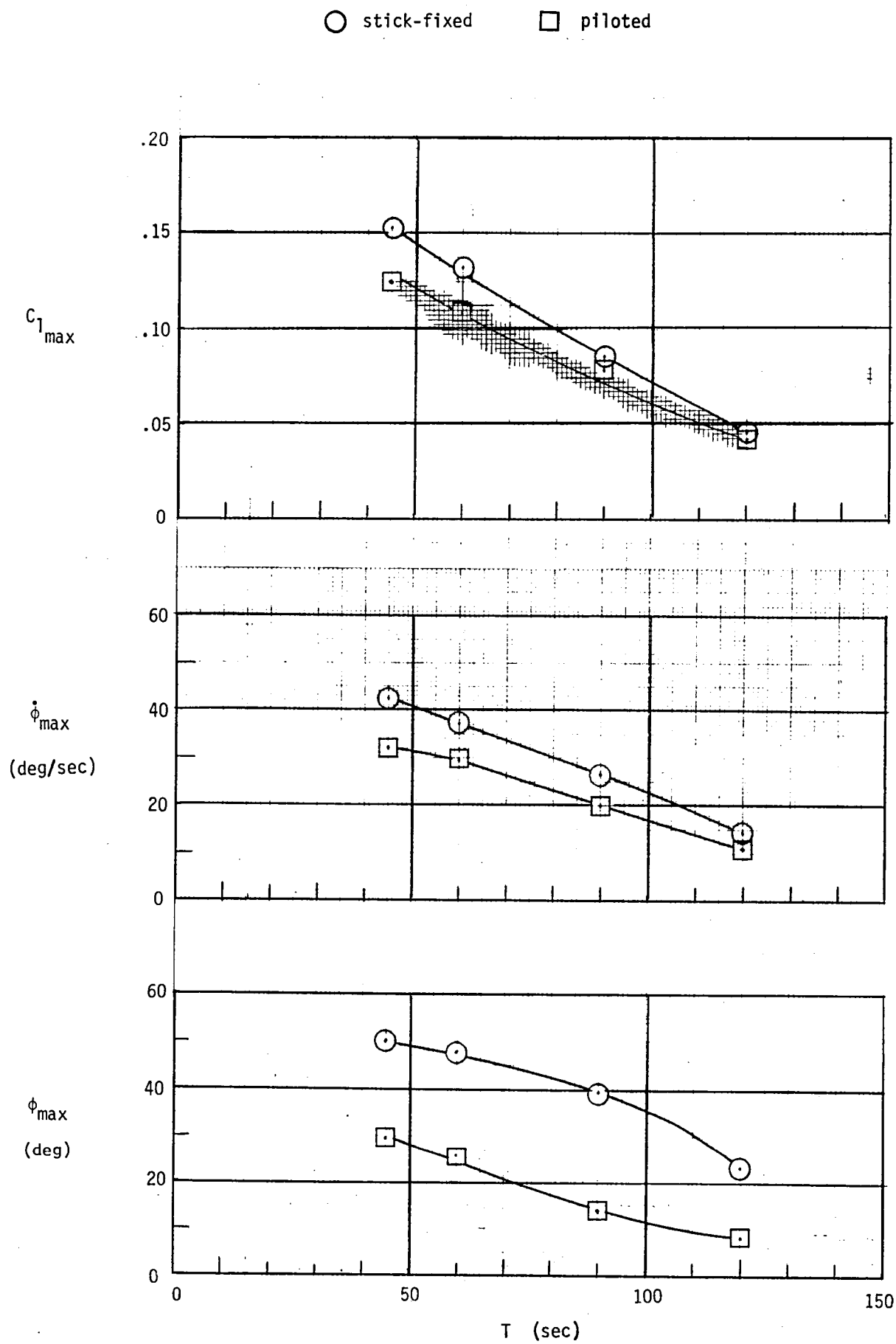

Figure 10.- Initial upset severity from baseline, in ground effect vortices.

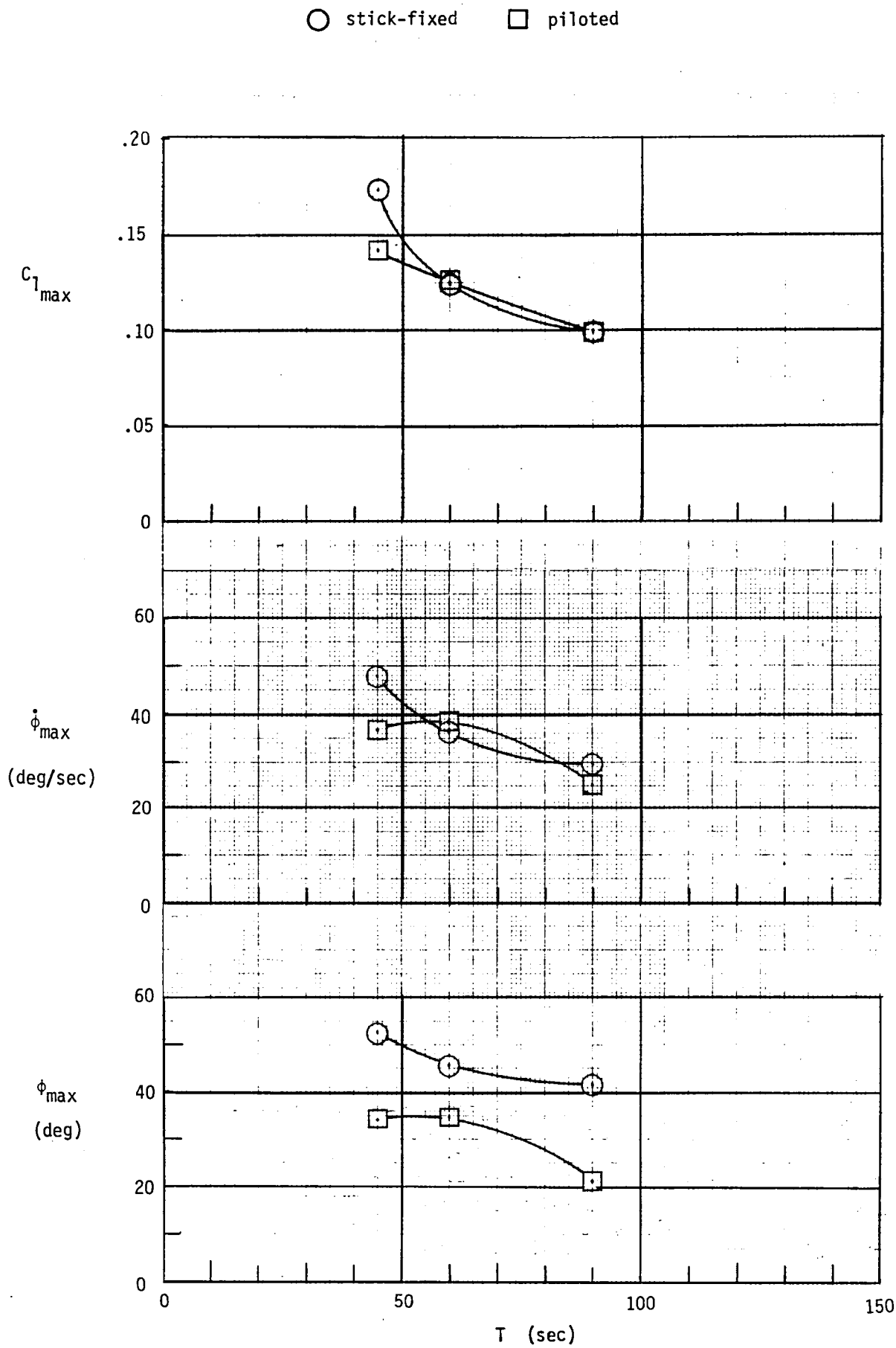

Figure 11.- Initial upset severity from attenuated (15^0 spoilers) vortices.

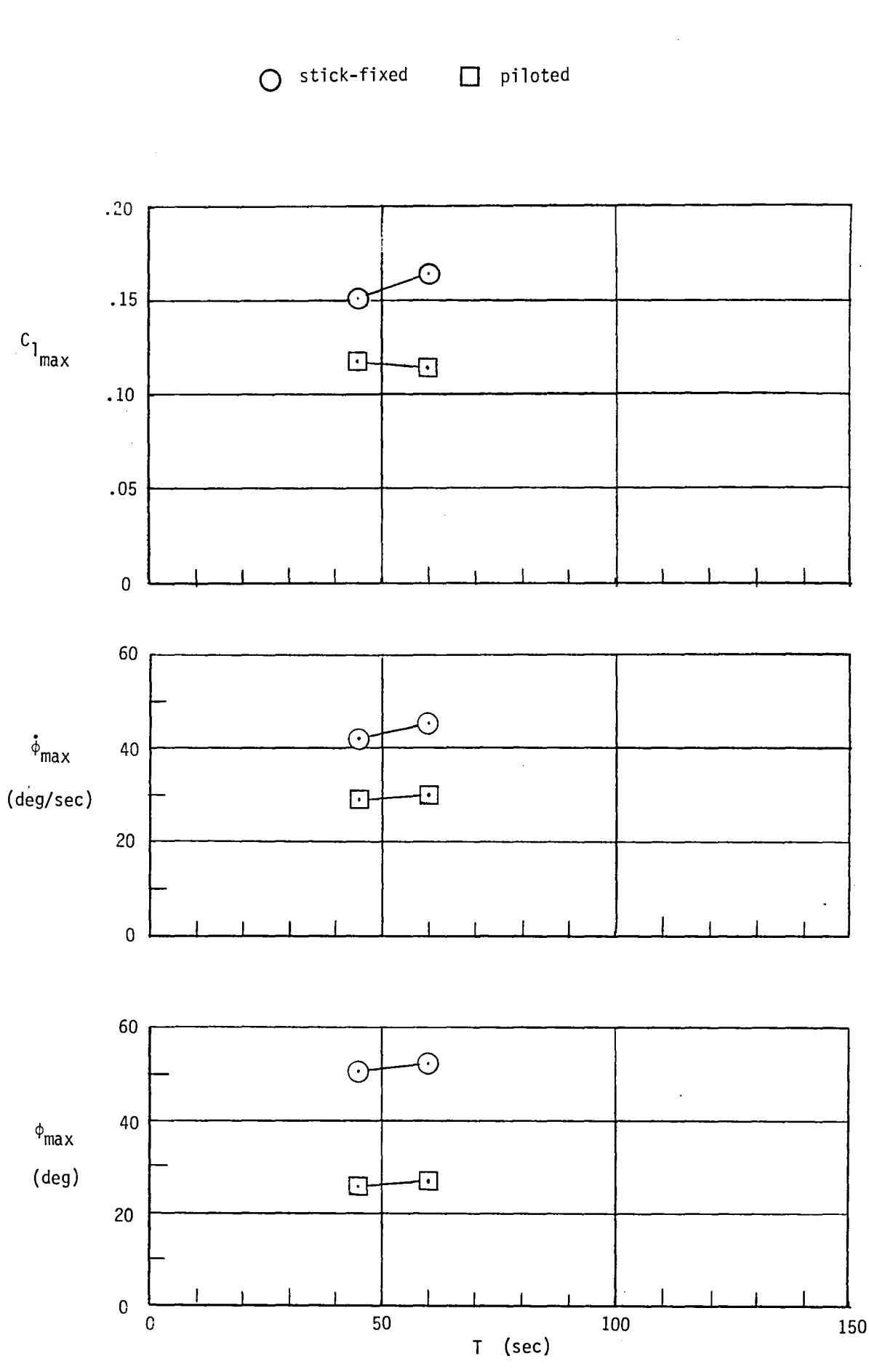

Figure 12.- Initial upset severity from attenuated (30^{o} spoilers) vortices.

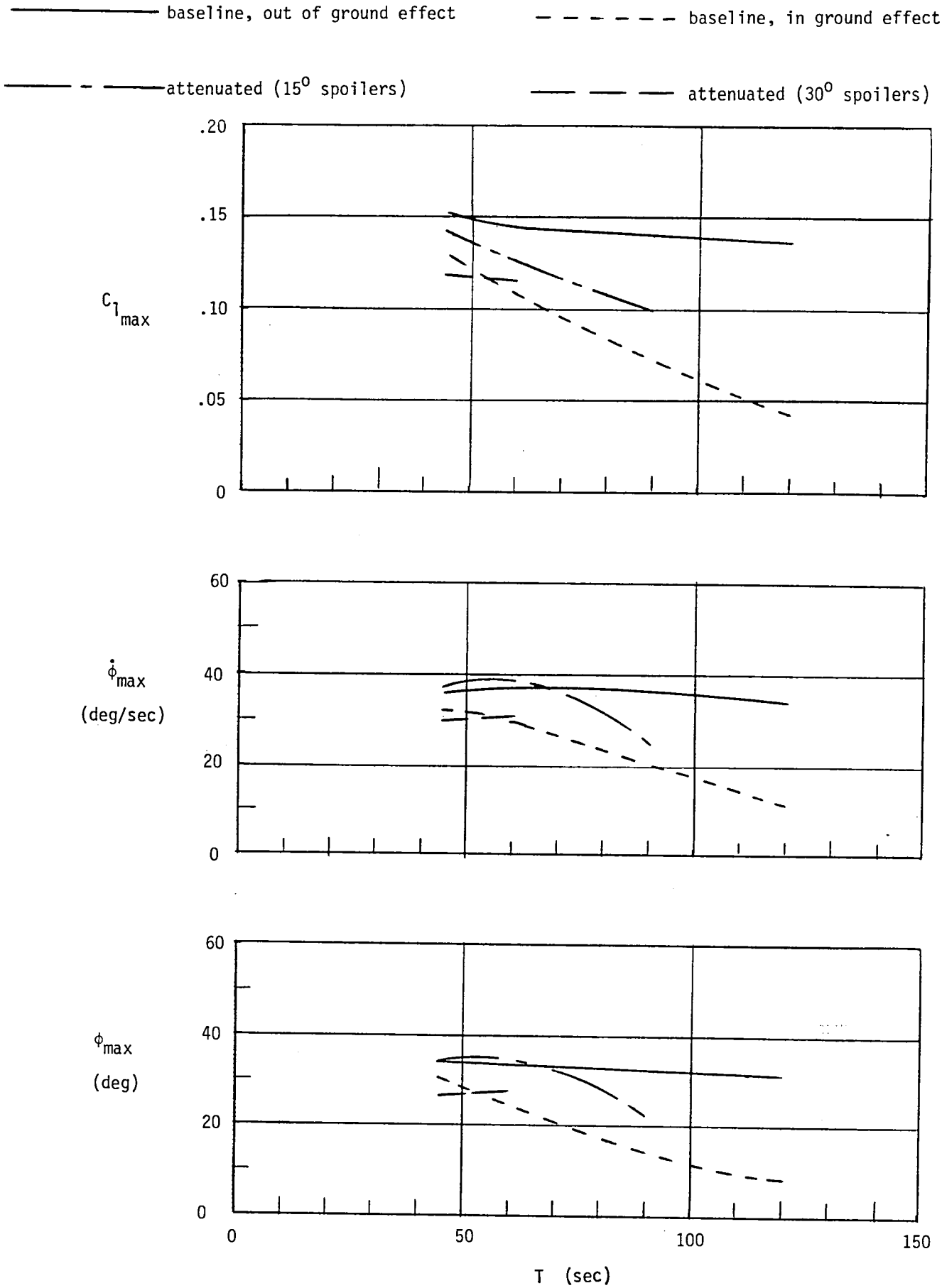

Figure 13.- Comparison of initial upset severity for piloted vortex encounters.

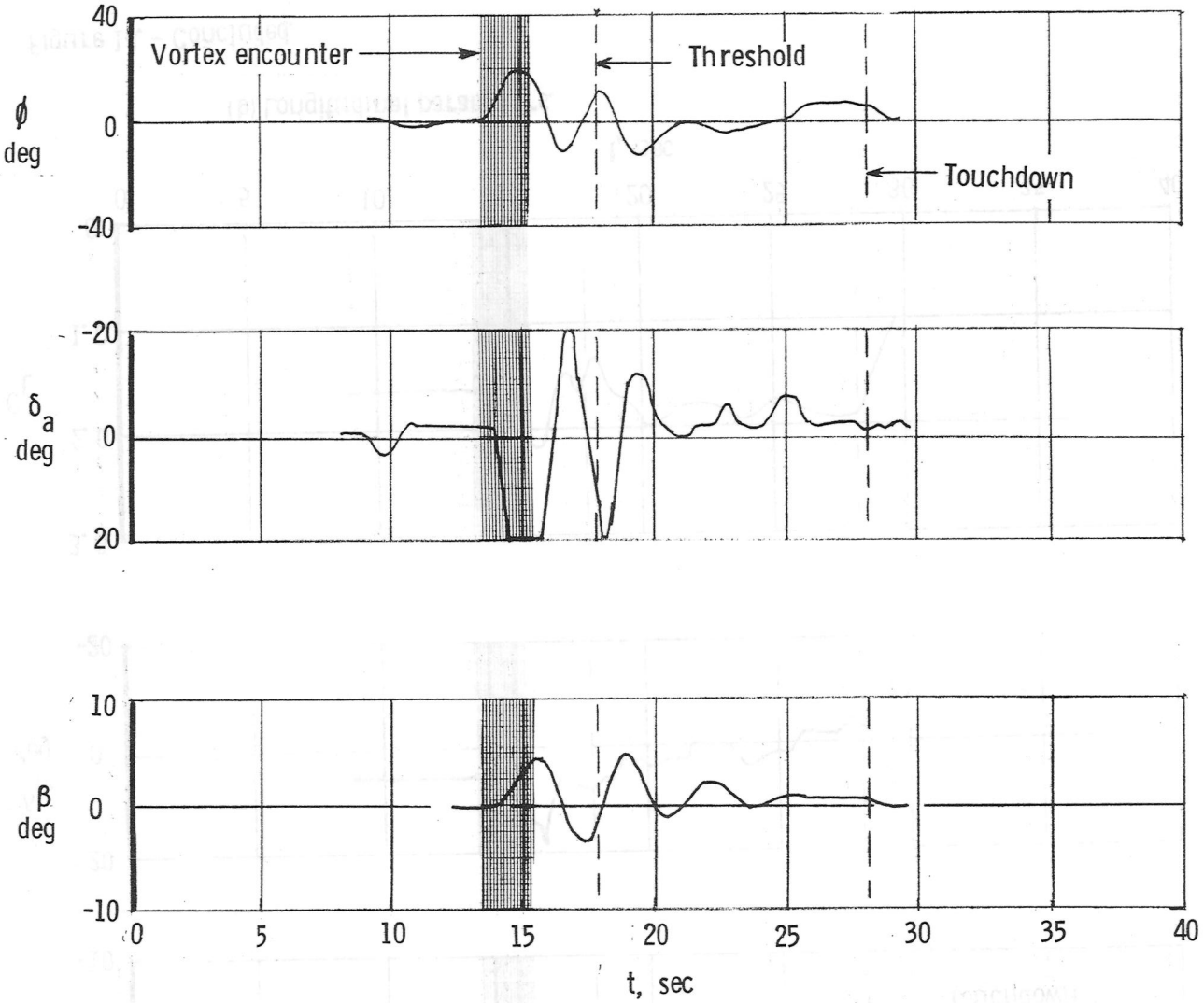

- Attenuated (15° spoilers) vortex
- Clockwise rotation
- T = 90 sec
- h_E = 30.5 m
- Y_E = 0.6 m

(a) Lateral-directional parameters.

Figure 14. - Time history of run 4.4.

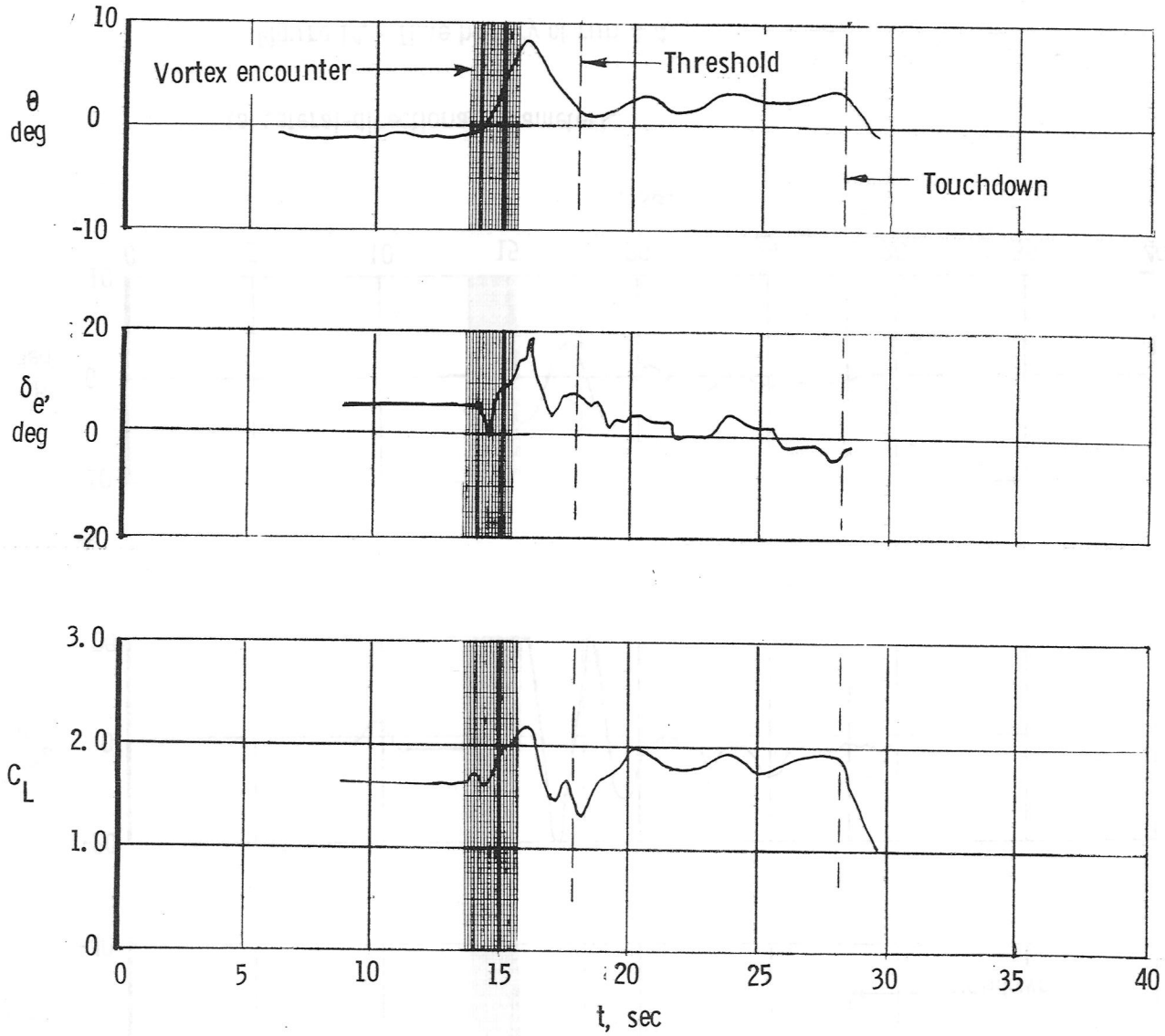

- Attenuated (15° spoilers) vortex
- Clockwise rotation
- T = 90 sec
- h_E = 30.5 m
- Y_E = 0.6 m

(b) Longitudinal parameters.

Figure 14. - Concluded.

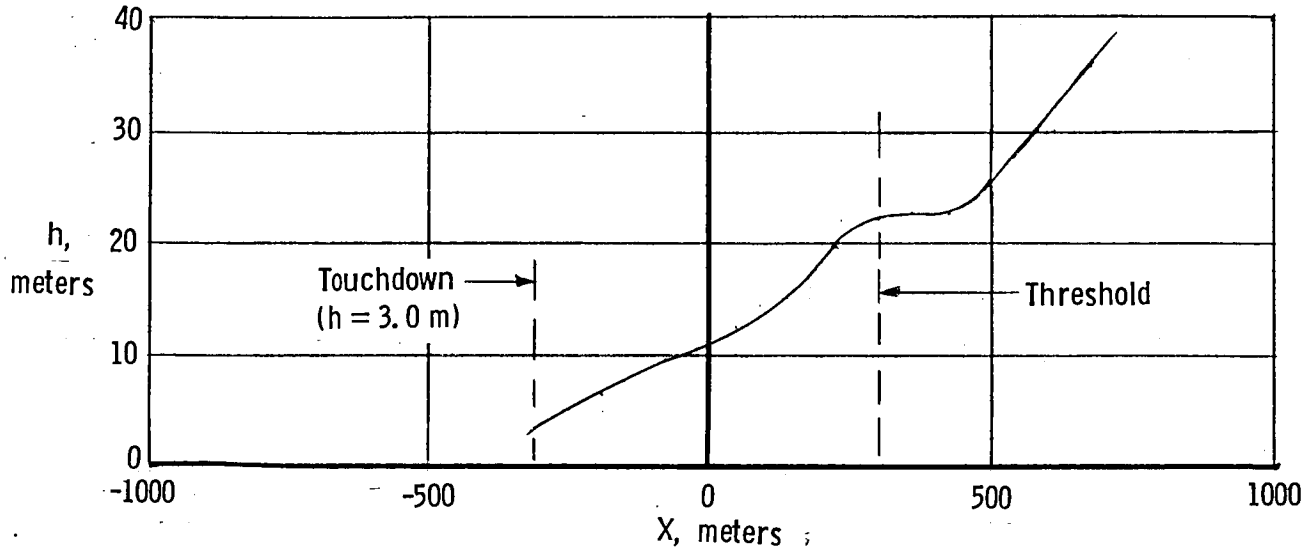

(a) Vertical projection.

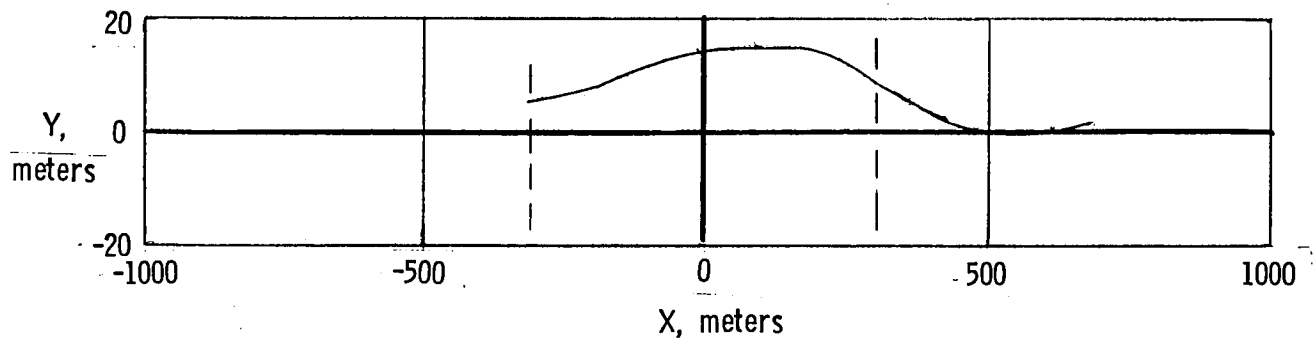

(b) Horizontal projection.

Figure 15. - Flight path for run 4.4.

Attenuated (15° spoiler) vortex
Clockwise rotation
T = 90 sec
h_E = 30.5 m
Y_E = 0.6 m

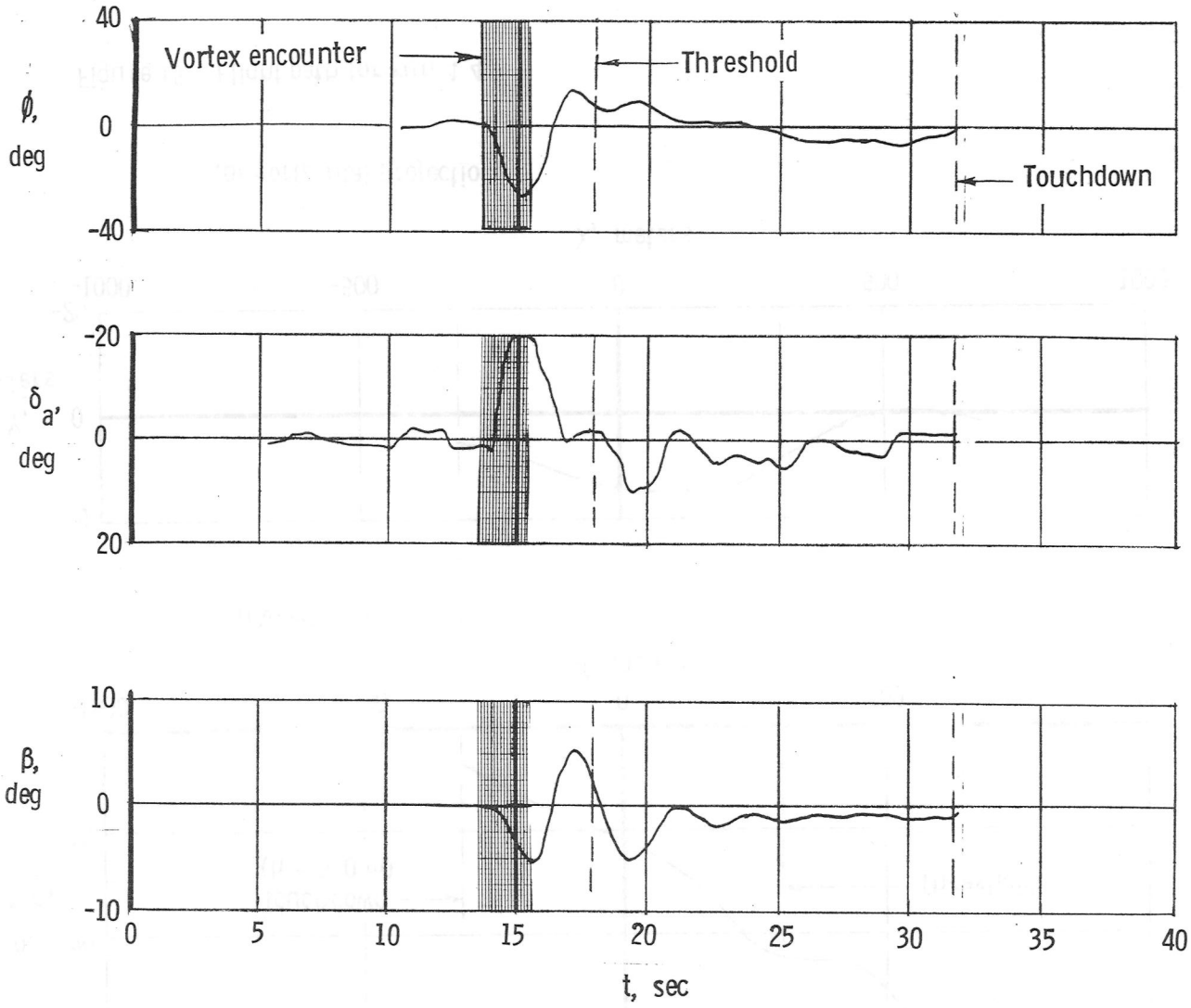

- Attenuated (15° spoilers) vortex
- Counter-clockwise rotation
- T = 60 sec
- h_e = 30.5 m
- Y_E = 2.71 m

(a) Lateral-directional parameters.

Figure 16. - Time history of run 4.13.

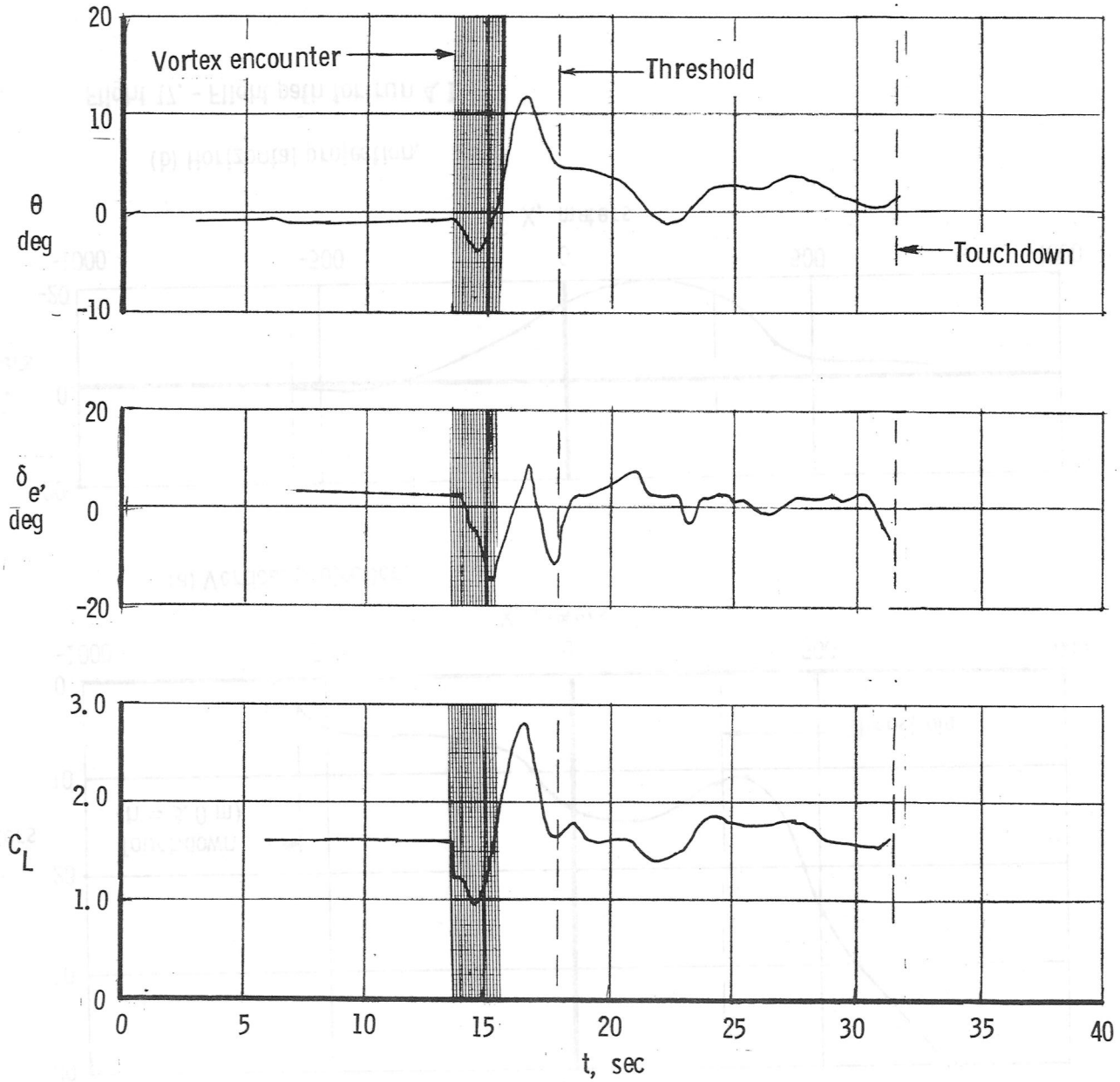

- Attenuated (15° spoilers) vortex
- Counter-clockwise rotation
- T = 60 sec
- h_e = 30.5 m
- Y_E = 2.71 m

(b) Longitudinal parameters.

Figure 16. - Concluded.

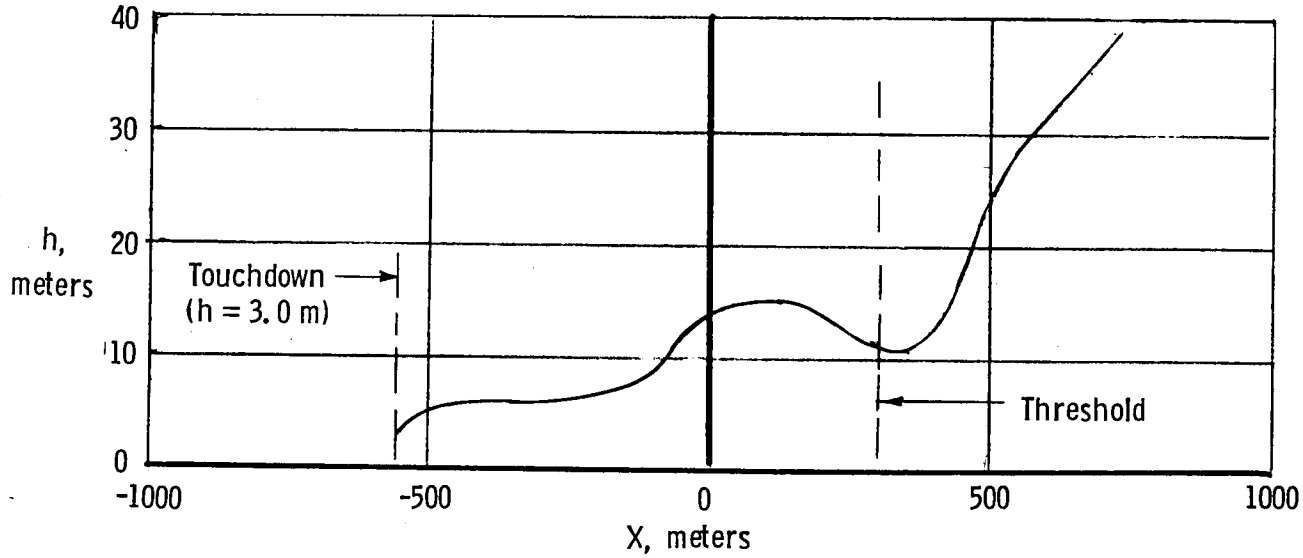

(a) Vertical projection.

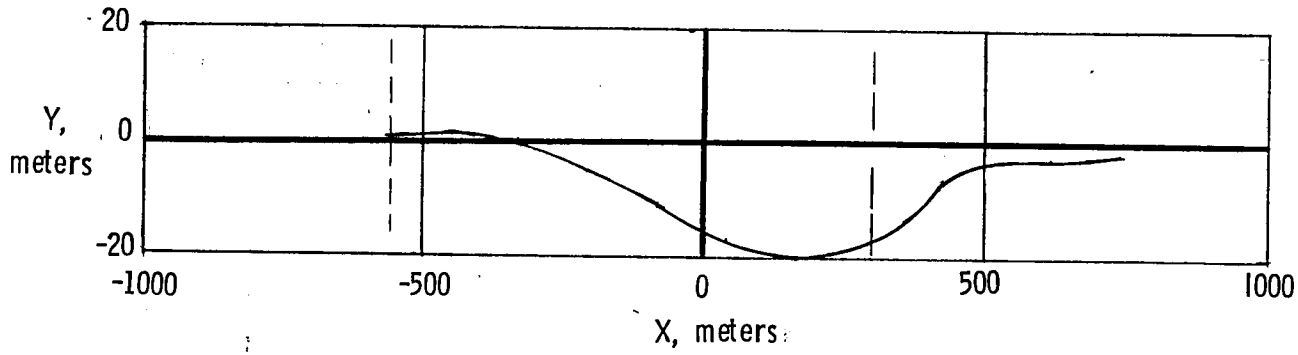

(b) Horizontal projection.

Flight 17. - Flight path for run 4.13.

Attenuated (15° spoilers) vortex
Counter-clockwise rotation
T = 60 sec
h_E = 30.5 m
Y_E = 2.71 m

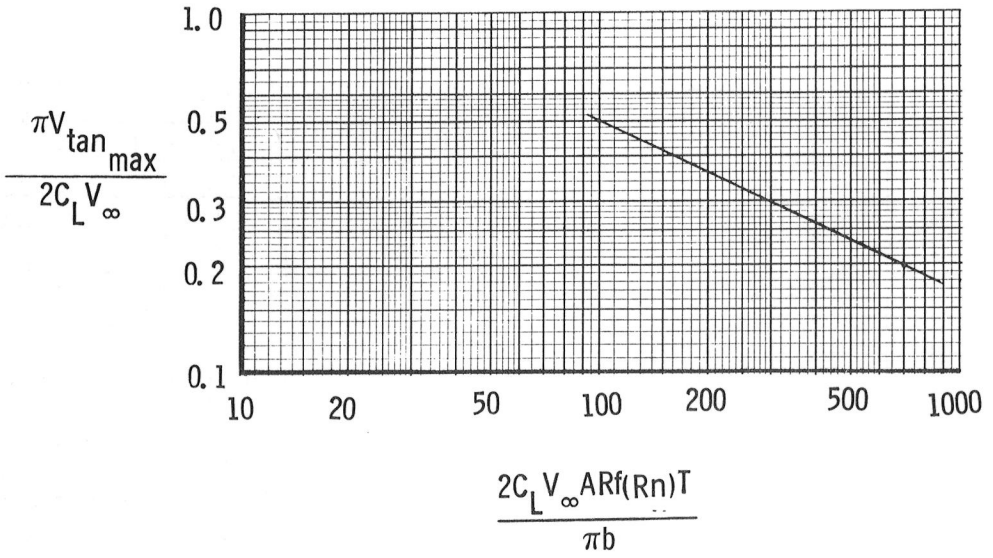

(a) Maximum tangential velocity.

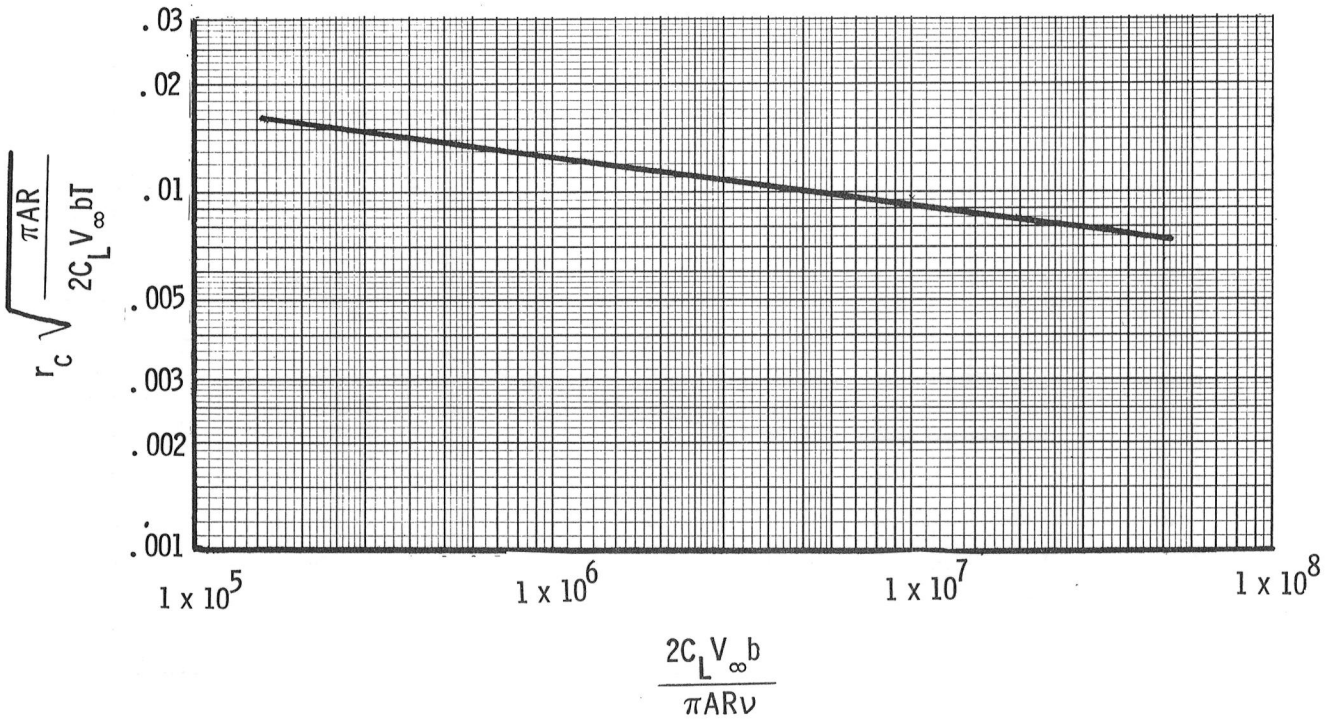

(b) Vortex core radius.

Figure 18. - Vortex modeling parameters- baseline vortex out of ground effect.

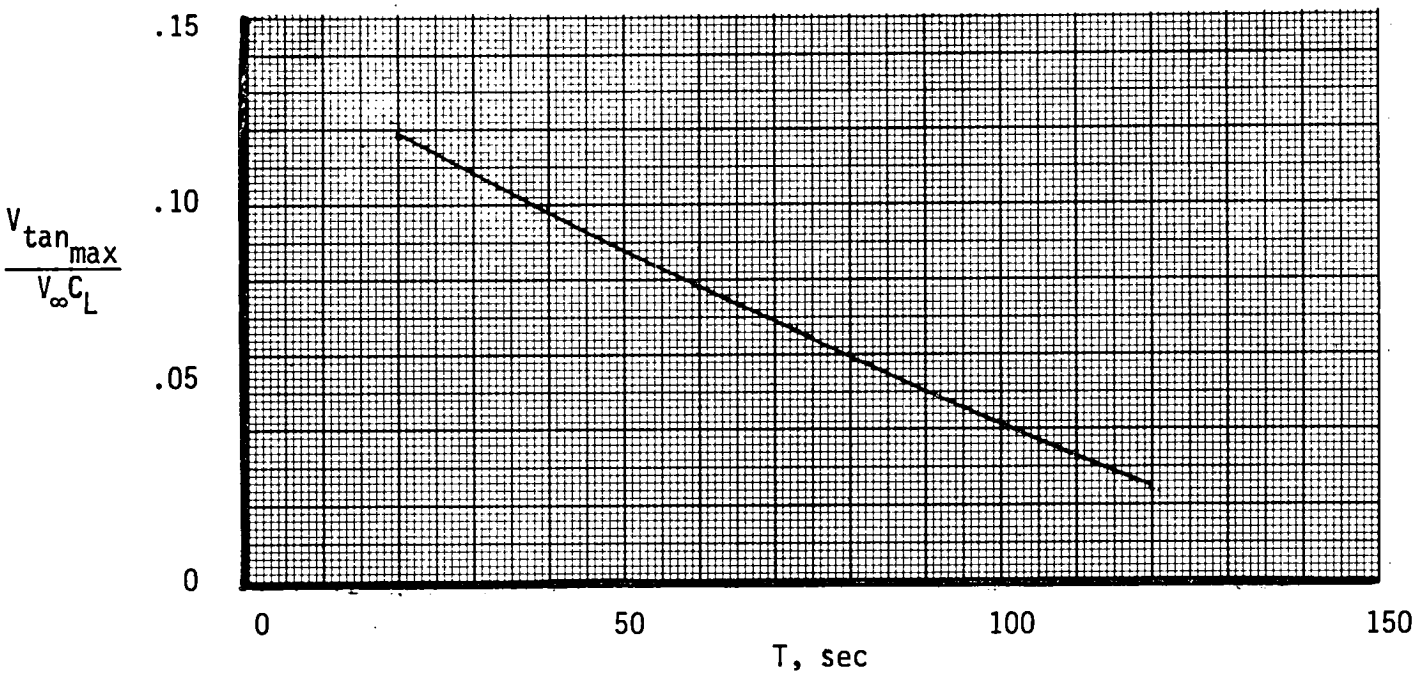

(a) maximum tangential velocity

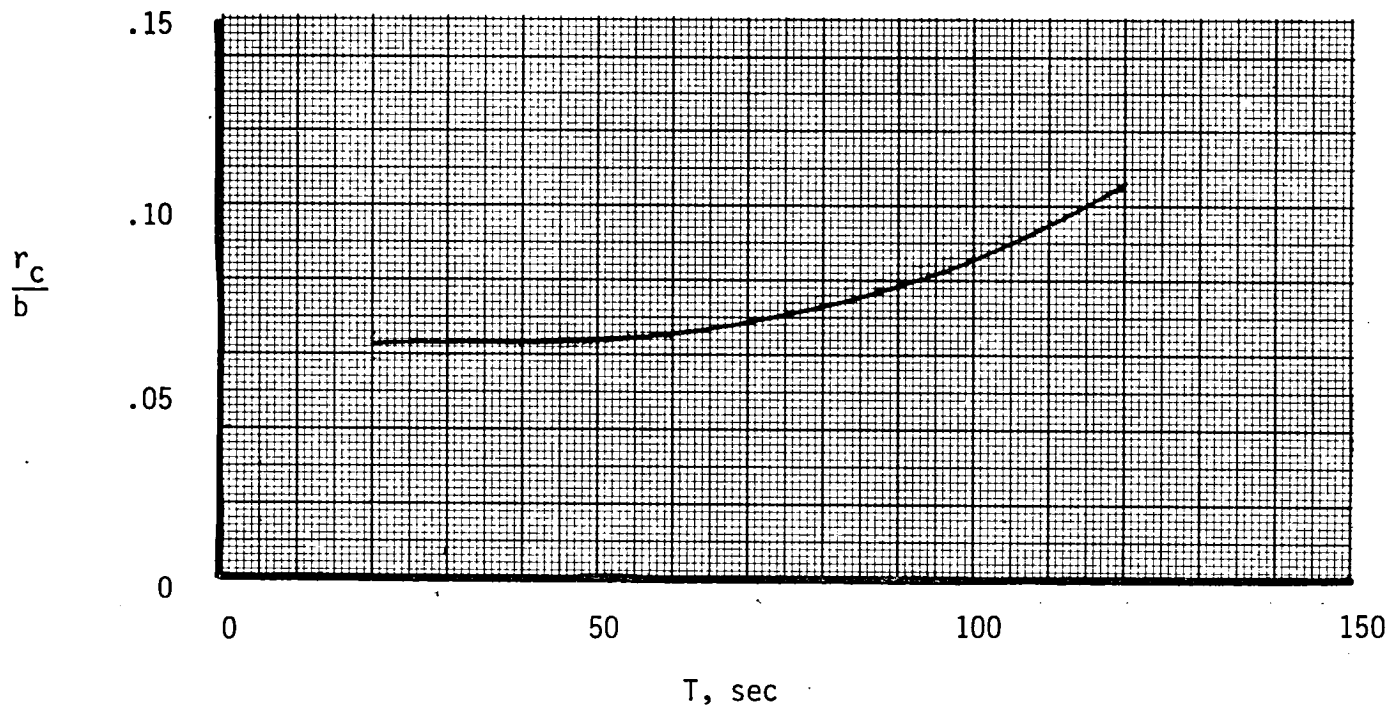

(b) vortex core radius

Figure 19.- Vortex modeling parameters--baseline vortex in ground effect.

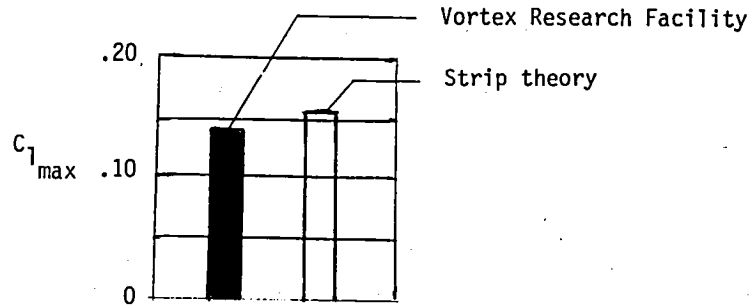

(a) Baseline vortex out-of-ground effect; separation interval of 0.88 nautical miles.

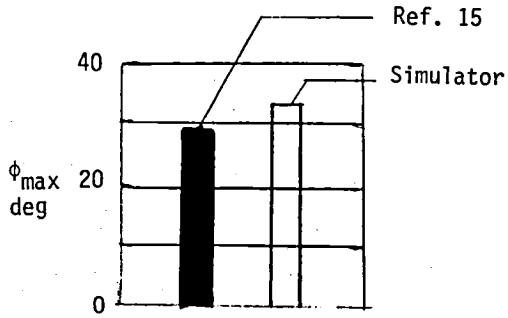

(b) Baseline vortex out-of-ground effect; separation interval of 3.0 nautical miles.

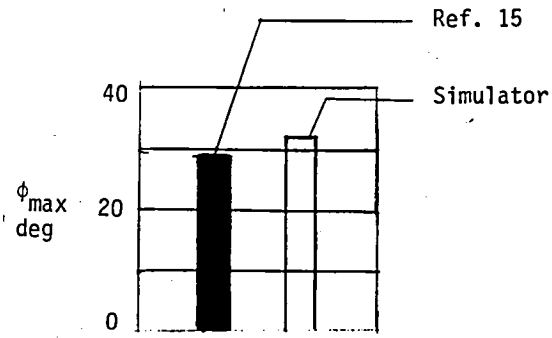

(c) Baseline vortex in ground effect; separation interval of 1.80 nautical miles.

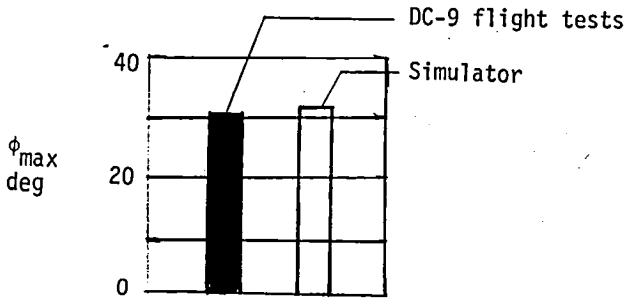

(d) Baseline vortex out-of-ground effect separation interval of 4.0 nautical miles.

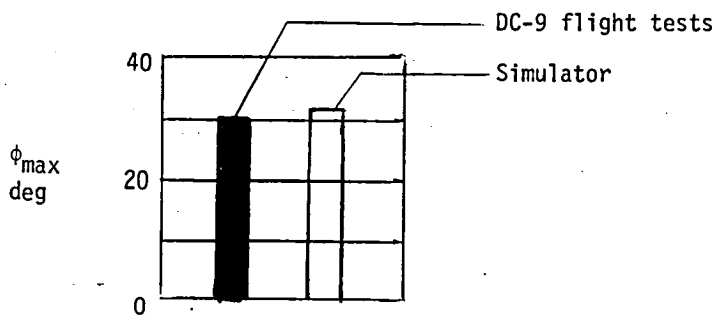

(e) Baseline vortex out-of-ground effect separation interval of 4.5 nautical miles.

Figure 20. - Comparison of maximum rolling moments and bank angles.

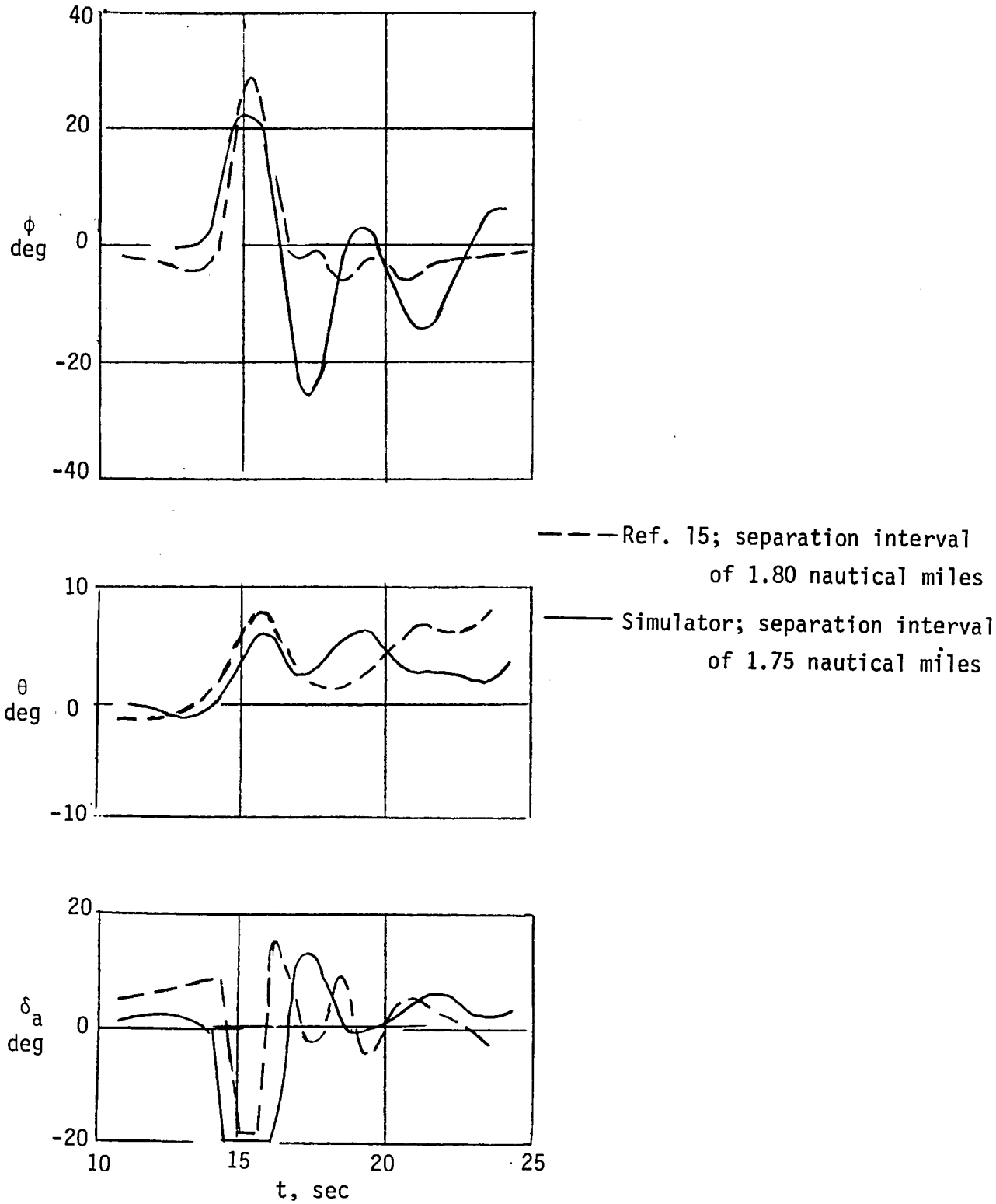

Figure 21.- Comparison of time histories from an encounter with a clockwise vortex in ground effect.

1. Report No.	2. Government Accession No.	3. Recipient's Catalog No.
NASA TM 81782		

4. Title and Subtitle	5. Report Date
Preliminary Results of Simulated Vortex Encounters by a Twin-Engine, Commercial Aircraft During Final Landing Approach	May 1980
	6. Performing Organization Code

7. Author(s)	8. Performing Organization Report No.
Earl C. Hastings, Jr., G. Thomas Holbrook, and Gerald L. Keyser, Jr.*	
	10. Work Unit No. 505-44-23-03
9. Performing Organization Name and Address NASA Langley Research Center Hampton, VA 23665	11. Contract or Grant No.
	13. Type of Report and Period Covered Technical Memorandum
12. Sponsoring Agency Name and Address National Aeronautics and Space Administration Washington, DC 20546	14. Sponsoring Agency Code

15. Supplementary Notes

*Gerald L. Keyser, Jr. (Major) (USAF), NASA Langley Research Center, Hampton, VA 23665
This paper provides supplementary data to SAE Paper No. 800775.

16. Abstract

Piloted simulations of encounters with vortices of various ages and degrees of attenuation were performed with the Visual Motion Simulator. In the simulations, a twin-engine, commercial transport on final approach, encountered the modeled vortices of a four-engine, wide-body, commercial transport. The data in this report show the effect of vortex age and attenuation on the severity of the initial upset, as well as the effect of the vortex encounters on the landing capability.

17. Key Words (Suggested by Author(s))	18. Distribution Statement
Vortex Encounters Vortex Characteristics Landing Capability Simulators	Unclassified - Unlimited 03 - Air Transportation and Safety

19. Security Classif. (of this report)	20. Security Classif. (of this page)	21. No. of Pages	22. Price*
Unclassified	Unclassified	54	$5.25

For sale by the National Technical Information Service, Springfield, Virginia 22161